CrossMark

Nonlinear Network Modes in Cyclic Systems with Applications to Connected Vehicles

Sergei S. Avedisov[1] · Gábor Orosz[1]

Abstract In this paper, we propose a novel technique to decompose networked systems with cyclic structure into nonlinear modes and apply these ideas to a system of connected vehicles. We perform linear and nonlinear transformations that exploit the network structure and lead to nonlinear modal equations that are decoupled. Each mode can be obtained by solving a small set of algebraic equations without deriving the coefficients for any other mode. By focusing on the mode that is loosing stability, bifurcation analysis can be carried out. The techniques developed are applied to evaluate the impact of connected cruise control on the nonlinear dynamics of a connected vehicle system.

1 Introduction

Ideas regarding using intelligent vehicles to improve the safety and efficiency of roadways originated in the 1930s, but early efforts were not successful due to the lack of inexpensive sensors. In the last two decades, more and more technologies have been

---

Communicated by Sue Ann Campbell.

✉ Sergei S. Avedisov
avediska@umich.edu

Gábor Orosz
orosz@umich.edu

[1]   Department of Mechanical Engineering, University of Michigan, Ann Arbor, MI 48109, USA

developed to increase safety and driver comfort (Shladover 1991), but mobility has not seen a similar transformation. Recent developments in wireless vehicle-to-vehicle (V2V) communication technologies may lead to a potential breakthrough at this front. These technologies allow vehicles to receive information about the surrounding traffic which may be used to assist human drivers and/or actuate the vehicles (Ge et al. 2013; Ge and Orosz 2014; Zhang and Orosz 2013). Indeed, the added communication layer increases the complexity of the arising connected vehicle systems, and thus, characterizing the impact of V2V control strategies on the system dynamics is a challenging task.

For example, one may exploit V2V communication to attenuate velocity fluctuations along the chain of vehicles in order to ensure the stability of the traffic flow. To achieve this, a strategy called connected cruise control (CCC) (Orosz 2014) may be used, which allows one to design decentralized controllers for individual vehicles receiving signals from multiple vehicles ahead. Understanding how CCC vehicles impact the overall traffic dynamics requires new mathematical methods that allow one to evaluate the dynamics of large connected systems when varying parameters (e.g., control gains). For the sake of simplicity, in this paper, we consider a simple setup where all the vehicles are equipped with CCC and each vehicle receives information from the vehicle immediately ahead. However, the mathematical tools developed here may be extended for more complicated communication topologies.

It is evident that CCC controllers must be nonlinear since the targeted velocity must be saturated at some minimum and maximum values. Consequently, we need to analyze the nonlinear dynamics of the arising connected vehicle systems. Of specific interest is to identify the domains of bistability in the parameter space where smooth traffic flow can be achieved, but sufficiently large perturbations may lead to stop-and-go traffic jams (Gasser et al. 2004; Helbing and Moussaid 2009; Orosz and Stépán 2006; Orosz et al. 2009). In Helbing and Moussaid (2009), the critical densities at which bistability appears were derived analytically for a simplified model, while nonlinear oscillatory solutions were characterized in Gasser et al. (2004) using Hopf calculations and numerical continuation. By extending these techniques to infinite-dimensional state spaces, the effects of driver reaction time were investigated in Orosz and Stépán (2006) and Orosz et al. (2009). While these techniques were successful when considering simplified human–driver models, they become cumbersome and inefficient when considering more complicated connected cruise control strategies. This demands new tools for the analysis of nonlinear networked systems to allow fast CCC prototyping where the control algorithms can be designed at the vehicle level, but their impact on the large-scale dynamics can also be evaluated.

One way to characterize nonlinear dynamics of high-dimensional systems is to identify the so-called nonlinear normal modes (NNMs). Here we briefly discuss the history of NNMs and refer the reader to the comprehensive summary presented in Kerschen et al. (2009). The concept of NNMs can be traced back to Rosenberg (1966), where he defined them as "vibrations-in-unison of the system". Shaw and Pierre expanded this definition in Shaw and Pierre (1993) to "a motion that takes place on a two-dimensional invariant manifold embedded in state space". (The manifold was two-dimensional since they were concerned about mechanical systems constructed of one-degree-of-freedom elements, but the concept can be generalized to higher-

dimensional manifolds.) By exploiting the invariance of these nonlinear manifolds, they presented an analytical method for the approximation of NNMs that led to algebraic equations. Other analytical techniques used to compute NNMs include various energy-based methods (Manevich and Mikhlin 1972; Rosenberg 1966); the method of multiple scales (Gendelman 2004; Nayfeh and Nayfeh 1994; Wang and Bajaj 2007); the method of normal forms (Jézéquel and Lamarque 1991; Nayfeh 1995); and the harmonic balance method (Haterbouch and Benamar 2005; Szemplinska-Stupnicka 1983). These analytical methods were applied to systems consisting of a small number of oscillators due to the complexity of the calculations.

In Kerschen et al. (2009), it was suggested that numerical continuation (Cochelin et al. 1994; Slater 1996) may be used to extend NNM analysis to systems containing larger numbers of oscillators. The practicality of continuation in NNM analysis was demonstrated in Peeters et al. (2009) along with several applications to mechanical systems, while in Georgiades et al. (2009) and Grolet and Thouverez (2010), continuation was used to obtain NNMs for structures with cyclic symmetry containing up to 60 oscillators. However, beyond this limit, numerical continuation becomes unfeasible due to high computational demand. Furthermore, when using numerical methods, one loses the intuition that can be gained when applying analytical approaches.

The analysis of networked systems with large numbers of nodes is not feasible with the current analytical and numerical methods since they lead to large numbers of coupled linear algebraic equations that need to be solved simultaneously to obtain the modal equations. Our goal is to extend these limitations by exploiting the network structure. Using network-based linear and nonlinear transformations, we decompose the system into uncoupled nonlinear modal equations. Each modal equation can be obtained by solving a small number of algebraic equations without considering the other modes. When bifurcations occur in the corresponding modal subspace, normal forms can be used to characterize the nonlinear behavior of the entire system.

In this paper, we present the mathematical methods for systems with cyclic structure and apply the developed tools to investigate the dynamics of a connected vehicle system where each vehicle is equipped with CCC and utilizes information about the motion of the vehicle immediately ahead; see Fig. 1a. The corresponding mathematical model is
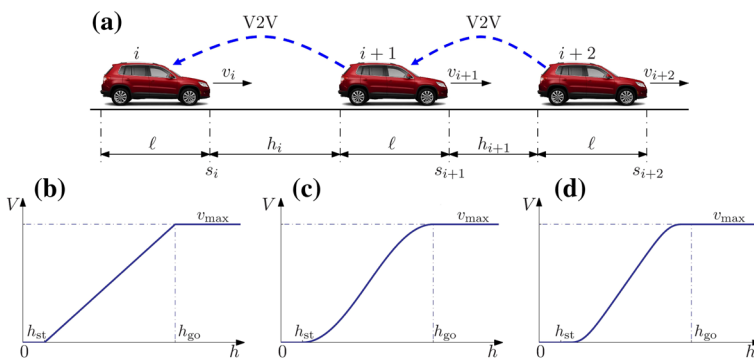

Fig. 1 **a** Connected vehicles traveling in a single lane with their kinematic properties indicated. **b–d** Range policies defined by (2) with their middle sections given by (3), (4), (5), respectively

Fig. 2 Directed graph arising through V2V communication on a circular road. The nodes (vehicles) in the system are depicted by *red dots*, and *dashed blue arrows* show the flow of V2V information between them. The *red arrow* indicates the direction of motion of vehicles along the road (Color figure online)
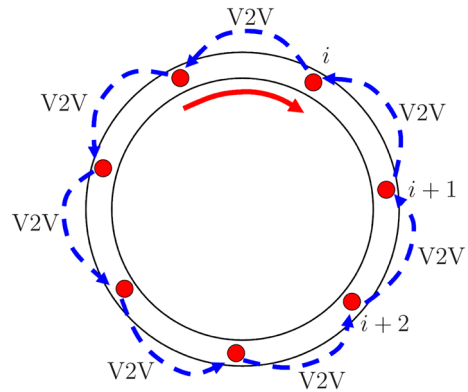
presented in Sect. 2. In Sect. 3, we develop a network-based algorithm for decomposing general systems with cyclic symmetry into nonlinear modes. In Sect. 4, we apply this algorithm to analyze nonlinear oscillations arising through a Hopf bifurcation in the connected vehicle system. Analytical results are compared to those of numerical continuation in Sect. 5, where we evaluate the effects of the CCC control parameters on the dynamics of the network. Finally, we discuss the implications of the network-based algorithms as well as future research directions in Sect. 6.

2 Modeling Framework

The model described in Orosz et al. (2011) and Orosz et al. (2010) is adopted here to motivate the nonlinear network-based analysis. We assume that identical vehicles travel on a single lane, and the i-th vehicle monitors the motion of the $i + 1$-st vehicle ahead using V2V communication; see Fig. 1a. The position of the i-th vehicle is denoted by s_i, its velocity is v_i, and ℓ represents the vehicle length. For simplicity, here we consider a controller that responds to the headway $h_i = s_{i+1} - s_i - \ell$ and the rate of change in headway $\dot{h}_i = v_{i+1} - v_i$ (also called relative velocity). The received information is used to actuate the vehicle according to

$$
\begin{aligned}
\dot{s}_i &= v_i, \\
\dot{v}_i &= \alpha \left(V(s_{i+1} - s_i - \ell) - v_i \right) + \beta \left(v_{i+1} - v_i \right),
\end{aligned}
\tag{1}
$$

where the gains $\alpha > 0$ and $\beta \geq 0$ are associated with the headway and relative velocity, respectively. In order to analyze the large-scale dynamics of the connected vehicle system, we place N cars on a circular road; see Fig. 2. In this configuration, the first vehicle follows the N-th vehicle, i.e., we have the periodic boundary conditions $s_{N+1} = s_1$, $v_{N+1} = v_1$, which result in an autonomous system. The total length of the road is $L + N\ell$, where L is called the effective road length. In this paper, we will use the average headway $h^* = L/N$ as the bifurcation parameter and present the results for different numbers of vehicles.

The headway feedback term in (1) involves the nonlinear function $V(h)$, which is called the range policy (or the optimal velocity function) and satisfies the following properties:

1. $V(h)$ is continuous and monotonically increasing (the more sparse the traffic is, the faster the vehicles want to travel).
2. $V(h) \equiv 0$ for $h \leq h_{\text{st}}$ (in dense traffic vehicles intend to stop).
3. $V(h) \equiv v_{\text{max}}$ for $h \geq h_{\text{go}}$ (in sparse traffic vehicles intend to travel with the maximum speed, also called the free-flow speed).

These properties can be summarized as

$$V(h) = \begin{cases} 0 & \text{if } h \leq h_{\text{st}}, \\ F(h) & \text{if } h_{\text{st}} < h < h_{\text{go}}, \\ v_{\text{max}} & \text{if } h \geq h_{\text{go}}, \end{cases} \tag{2}$$

where $F(h)$ is strictly monotonically increasing such that $F(h_{\text{st}}) = 0$, $F(h_{\text{go}}) = v_{\text{max}}$. For instance, the range policies with functions

$$F(h) = v_{\text{max}} \frac{h - h_{\text{st}}}{h_{\text{go}} - h_{\text{st}}}, \tag{3}$$

$$F(h) = \frac{v_{\text{max}}}{2} \left[1 - \cos \left(\pi \frac{h - h_{\text{st}}}{h_{\text{go}} - h_{\text{st}}} \right) \right], \tag{4}$$

$$F(h) = \frac{v_{\text{max}}}{2} \left[1 + \tanh \left(\tan \left(\frac{\pi}{2} \cdot \frac{2h - h_{\text{go}} - h_{\text{st}}}{h_{\text{go}} - h_{\text{st}}} \right) \right) \right], \tag{5}$$

are shown in Fig. 1b–d. We remark that the analytical calculations presented in this paper do not require a specific range policy. When comparing the analytical results to numerical ones, we will use the function (4), but any function satisfying the properties 1–3 would result in similar qualitative results.

One can show that (1) admits a pseudo-equilibrium state where all cars are equidistant and travel with the same velocity, that is,

$$s_i^* = v_i^* t + s_i^0, \quad i = 1, \ldots, N, \tag{6}$$

such that

$$\begin{aligned} s_{i+1}^0 - s_i^0 - \ell &= \frac{L}{N} = h^*, \quad i = 1, \ldots, N - 1, \\ s_1^0 - s_N^0 - \ell &= \frac{L}{N} = h^*, \\ v_i^* = v^* &= V(h^*), \quad i = 1, \ldots, N. \end{aligned} \tag{7}$$

We define the perturbations

$$\widetilde{s}_i = s_i - s_i^*, \quad \widetilde{v}_i = v_i - v^*, \tag{8}$$

and approximate the system about the pseudo-equilibrium (6, 7) up to the cubic order using Taylor expansion that yields

$$\dot{\widetilde{s}}_i = \widetilde{v}_i,$$
$$\dot{\widetilde{v}}_i = p\,(\widetilde{s}_{i+1} - \widetilde{s}_i) + \frac{q}{2}(\widetilde{s}_{i+1} - \widetilde{s}_i)^2 + \frac{r}{6}(\widetilde{s}_{i+1} - \widetilde{s}_i)^3 + \beta\,(\widetilde{v}_{i+1} - \widetilde{v}_i) - \alpha\,\widetilde{v}_i, \tag{9}$$

where

$$p = \alpha\,V'(h^*),$$
$$q = \alpha\,V''(h^*), \tag{10}$$
$$r = \alpha\,V'''(h^*),$$

and the prime denotes the derivative with respect to the headway h.

   The system (1) for $i = 1, \dots, N$ consists of $2N$ equations and the same holds for the approximation (9) for $i = 1, \dots, N$. Thus, the nonlinear analysis by traditional center manifold reduction is demanding for large N. However, the system possesses a cyclic ($\mathbb{Z}_N$) symmetry that may be exploited when analyzing the nonlinear dynamics.

3 Nonlinear Network-Based Analysis

In this section, we develop methods for the nonlinear analysis of a general system with cyclic structure. For simplicity, we present the result for two equations per node and unidirectional nearest-neighbor coupling, but the approach can be generalized for arbitrary number of equations per node and more general coupling structures that admit $\mathbb{Z}_N$ symmetry. We investigate the system in the vicinity of a uniform equilibrium, where we approximate the dynamics using Taylor expansion up to third order. We then write the quadratic and cubic terms of the approximated system into a compact form, which allows us to perform a series of linear and nonlinear network-based transformations. These transformations result in nonlinear modal equations that are decoupled and can be analyzed separately in order to characterize the dynamics of the entire system.

   Consider a system composed of N nodes arranged in a cyclic structure where the $i + 1$-st node is connected to the i-th node and the first node is connected to the N-th node; see Fig. 2. Assuming that the state of the i-th node is described by the vector $\mathbf{x}_i = [x_i^{(1)}\ x_i^{(2)}]^{\mathrm{T}}$, where T denotes the transpose, the dynamics of the i-th node can be written into the form

$$\dot{\mathbf{x}}_i = \mathbf{g}(\mathbf{x}_i, \mathbf{x}_{i+1}), \tag{11}$$

for $i = 1, \dots, N$, where $\mathbf{g} = [g^{(1)}\ g^{(2)}]^{\mathrm{T}}$ and $\mathbf{x}_{N+1} \equiv \mathbf{x}_1$. We assume that the system possesses a uniform equilibrium

$$\mathbf{x}_i^* = \mathbf{x}^*, \tag{12}$$

for $i = 1, \dots, N$ which satisfies $\mathbf{g}(\mathbf{x}^*, \mathbf{x}^*) = 0$.

   By defining the perturbation

$$\mathbf{y}_i = \mathbf{x}_i - \mathbf{x}^*, \tag{13}$$

where $\mathbf{y}_i = [y_i^{(1)} \ y_i^{(2)}]^{\mathrm{T}}$, the third-order Taylor approximation of (11) around the equilibrium (12) can be written as

$$
\begin{aligned}
\dot{\mathbf{y}}_i = {} & [\mathfrak{J}_0]^* \mathbf{y}_i + [\mathfrak{J}_1]^* \mathbf{y}_{i+1} + \frac{1}{2} \sum_{b=0,1} \sum_{\beta=1,2} \mathbf{H}_b^{(\beta)}(\mathbf{y}_{i+b}) \Big([\partial_b^{(\beta)} \mathfrak{J}_0]^* \mathbf{y}_i + [\partial_b^{(\beta)} \mathfrak{J}_1]^* \mathbf{y}_{i+1} \Big) \\
& + \frac{1}{6} \sum_{b=0,1} \sum_{\beta=1,2} \sum_{d=0,1} \sum_{\delta=1,2} \mathbf{H}_b^{(\beta)}(\mathbf{y}_{i+b}) \, \mathbf{H}_d^{(\delta)}(\mathbf{y}_{i+d}) \qquad\qquad (14) \\
& \times \Big([\partial_b^{(\beta)} \partial_d^{(\delta)} \mathfrak{J}_0]^* \mathbf{y}_i + [\partial_b^{(\beta)} \partial_d^{(\delta)} \mathfrak{J}_1]^* \mathbf{y}_{i+1} \Big),
\end{aligned}
$$

where $\partial_b^{(\beta)} = \frac{\partial}{\partial x_{i+b}^{(\beta)}}$, and the operators

$$
\mathfrak{J}_b = \begin{bmatrix} \partial_b^{(1)} g^{(1)} & \partial_b^{(2)} g^{(1)} \\ \partial_b^{(1)} g^{(2)} & \partial_b^{(2)} g^{(2)} \end{bmatrix}, \qquad\qquad (15)
$$

where $b = 0, 1$ represent the derivatives of the function $\mathbf{g}$. In (14), the asterisk denotes that the derivatives are evaluated at the equilibrium. The quadratic and cubic terms contain the diagonal matrices

$$
\mathbf{H}_b^{(\beta)}(\mathbf{y}_i) = \begin{bmatrix} y_{i+b}^{(\beta)} & 0 \\ 0 & y_{i+b}^{(\beta)} \end{bmatrix}, \qquad\qquad (16)
$$

for $\beta = 1, 2$, $b = 0, 1$, and $i = 1, \ldots, N$. The matrix $\mathbf{H}_0^{(\beta)}(\mathbf{y}_i)$ is related to the self-feedback (the dependence of a node's dynamics on its own states), while $\mathbf{H}_1^{(\beta)}(\mathbf{y}_{i+1})$ is related to the coupling (the dependence of a node's dynamics on the state of the neighboring node). We remark that the double sum in (14) results in four different quadratic terms, while the quadruple sum results in 10 different cubic terms.

3.1 Network Structure

Before we proceed with the general analysis, we rewrite (14) into a form that allows us to take advantage of the cyclic structure during the linear and nonlinear analysis. In order to do this, we first define the direct product (or Kronecker product) of matrices $\mathbf{B} = [b_{ij}] \in \mathbb{C}^{N \times M}$ and $\mathbf{C} \in \mathbb{C}^{P \times Q}$ as

$$
\mathbf{B} \otimes \mathbf{C} = \begin{bmatrix} b_{11}\mathbf{C} & b_{12}\mathbf{C} & \cdots & b_{1M}\mathbf{C} \\ b_{21}\mathbf{C} & b_{22}\mathbf{C} & \cdots & b_{2M}\mathbf{C} \\ \vdots & \vdots & \ddots & \vdots \\ b_{N1}\mathbf{C} & b_{N2}\mathbf{C} & \cdots & b_{NM}\mathbf{C} \end{bmatrix}, \qquad\qquad (17)
$$

where $\mathbf{B} \otimes \mathbf{C} \in \mathbb{C}^{NP \times MQ}$. We also define the vector $\hat{\mathbf{y}} = \mathrm{col}[\mathbf{y}_1 \ \cdots \ \mathbf{y}_i \ \cdots \ \mathbf{y}_N]$, where the operator $\mathrm{col}[\cdot]$ stacks vectors into one large column vector. Thus, using (14) and (17), the dynamics of the entire system can be written into the form

$$\dot{\mathbf{y}} = \left(\mathbf{I}_N \otimes [\mathfrak{J}_0]^* + \mathbf{A}_N \otimes [\mathfrak{J}_1]^*\right)\hat{\mathbf{y}} + \frac{1}{2}\sum_{b=0,1}\sum_{\beta=1,2}\hat{\mathfrak{L}}^{(\beta)}(\hat{\mathbf{H}}_b(\hat{\mathbf{y}}))\left(\mathbf{I}_N \otimes [\partial_b^{(\beta)}\mathfrak{J}_0]^*\right.$$

$$+ \left.\mathbf{A}_N \otimes [\partial_b^{(\beta)}\mathfrak{J}_1]^*\right)\hat{\mathbf{y}}$$

$$+ \frac{1}{6}\sum_{b=0,1}\sum_{\beta=1,2}\sum_{d=0,1}\sum_{\delta=1,2}\hat{\mathfrak{L}}^{(\beta)}(\hat{\mathbf{H}}_b(\hat{\mathbf{y}}))\hat{\mathfrak{L}}^{(\delta)}(\hat{\mathbf{H}}_d(\hat{\mathbf{y}}))\left(\mathbf{I}_N \otimes [\partial_b^{(\beta)}\partial_d^{(\delta)}\mathfrak{J}_0]^*\right.$$

$$+ \left.\mathbf{A}_N \otimes [\partial_b^{(\beta)}\partial_d^{(\delta)}\mathfrak{J}_1]^*\right)\hat{\mathbf{y}}, \tag{18}$$

where $\mathbf{I}_N$ is the N-dimensional identity matrix and $\mathbf{A}_N = [\,a_{ij}\,]$ is the N-dimensional adjacency matrix with circulant structure, whose elements are defined as

$$a_{ij} = \begin{cases} 1 & \text{if } j = i + 1, \\ 0 & \text{otherwise.} \end{cases} \tag{19}$$

As mentioned above, for $i = N$, we have $j = 1$. The Jacobian matrix in (18) contains the blocks $[\mathfrak{J}_0]^*$ along the diagonal and the blocks $[\mathfrak{J}_1]^*$ above the diagonal representing the self-coupling and the effects of the neighbors, respectively.

The nonlinear self-feedback terms feature the $2N$-dimensional diagonal matrix

$$\hat{\mathbf{H}}_0(\hat{\mathbf{y}}) = \text{diag}\left(\begin{bmatrix} y_i^{(1)} & 0 \\ 0 & y_i^{(2)} \end{bmatrix}\right), \tag{20}$$

where the operator $\text{diag}(\cdot)$ is defined by

$$\text{diag}(\mathbf{B}_i) = \text{diag}(\mathbf{B}_1, \mathbf{B}_2, \ldots, \mathbf{B}_N) = \begin{bmatrix} \mathbf{B}_1 & \mathbf{0} & \ldots & \mathbf{0} \\ \mathbf{0} & \mathbf{B}_2 & \ldots & \mathbf{0} \\ \vdots & \vdots & \ddots & \vdots \\ \mathbf{0} & \mathbf{0} & \ldots & \mathbf{B}_N \end{bmatrix}, \tag{21}$$

as adopted from Olson et al. (2014). To be able to represent the nonlinear coupling terms, we shift the blocks along the diagonal in a circulant manner using

$$\hat{\mathbf{H}}_1(\hat{\mathbf{y}}) = (\mathbf{A}_N \otimes \mathbf{I})\,\hat{\mathbf{H}}_0(\hat{\mathbf{y}})\,(\mathbf{A}_N^{-1} \otimes \mathbf{I}) = \text{diag}\left(\begin{bmatrix} y_{i+1}^{(1)} & 0 \\ 0 & y_{i+1}^{(2)} \end{bmatrix}\right), \tag{22}$$

where $\mathbf{I}$ is the two-dimensional identity matrix. Matrices (20) and (22) are the basic building blocks for the quadratic and cubic terms for the system dynamics. To be able to express all possible terms, we shuffle the variables within the blocks of $\hat{\mathbf{H}}_0(\hat{\mathbf{y}})$ and $\hat{\mathbf{H}}_1(\hat{\mathbf{y}})$. First, we define two linear shuffling operators $\mathfrak{L}^{(1)}$ and $\mathfrak{L}^{(2)}$ whose action on the diagonal matrix

$$\mathbf{M} = \begin{bmatrix} \mu & 0 \\ 0 & \upsilon \end{bmatrix}, \tag{23}$$

is given by

$$
\begin{aligned}
\mathcal{L}^{(1)}(\mathbf{M}) &= \begin{bmatrix} 1 & 0 \\ 0 & 0 \end{bmatrix} \mathbf{M} \begin{bmatrix} 1 & 0 \\ 0 & 0 \end{bmatrix} + \begin{bmatrix} 0 & 0 \\ 1 & 0 \end{bmatrix} \mathbf{M} \begin{bmatrix} 0 & 1 \\ 0 & 0 \end{bmatrix} = \begin{bmatrix} \mu & 0 \\ 0 & \mu \end{bmatrix}, \\
\mathcal{L}^{(2)}(\mathbf{M}) &= \begin{bmatrix} 0 & 0 \\ 0 & 1 \end{bmatrix} \mathbf{M} \begin{bmatrix} 0 & 0 \\ 0 & 1 \end{bmatrix} + \begin{bmatrix} 0 & 1 \\ 0 & 0 \end{bmatrix} \mathbf{M} \begin{bmatrix} 0 & 0 \\ 1 & 0 \end{bmatrix} = \begin{bmatrix} \upsilon & 0 \\ 0 & \upsilon \end{bmatrix}.
\end{aligned}
\tag{24}
$$

Consequently, considering a block matrix $\hat{\mathbf{M}} \in \mathbb{C}^{2N \times 2N}$ with 2×2 diagonal blocks

$$\hat{\mathbf{M}}_{ij} = \begin{bmatrix} \mu_{ij} & 0 \\ 0 & \upsilon_{ij} \end{bmatrix}, \tag{25}$$

we can define the shuffling operators

$$
\begin{aligned}
\hat{\mathfrak{L}}^{(1)}(\hat{\mathbf{M}}) &= \left(\mathbf{I}_N \otimes \begin{bmatrix} 1 & 0 \\ 0 & 0 \end{bmatrix} \right) \hat{\mathbf{M}} \left(\mathbf{I}_N \otimes \begin{bmatrix} 1 & 0 \\ 0 & 0 \end{bmatrix} \right) \\
&\quad + \left(\mathbf{I}_N \otimes \begin{bmatrix} 0 & 0 \\ 1 & 0 \end{bmatrix} \right) \hat{\mathbf{M}} \left(\mathbf{I}_N \otimes \begin{bmatrix} 0 & 1 \\ 0 & 0 \end{bmatrix} \right), \\
\hat{\mathfrak{L}}^{(2)}(\hat{\mathbf{M}}) &= \left(\mathbf{I}_N \otimes \begin{bmatrix} 0 & 0 \\ 0 & 1 \end{bmatrix} \right) \hat{\mathbf{M}} \left(\mathbf{I}_N \otimes \begin{bmatrix} 0 & 0 \\ 0 & 1 \end{bmatrix} \right) \\
&\quad + \left(\mathbf{I}_N \otimes \begin{bmatrix} 0 & 1 \\ 0 & 0 \end{bmatrix} \right) \hat{\mathbf{M}} \left(\mathbf{I}_N \otimes \begin{bmatrix} 0 & 0 \\ 1 & 0 \end{bmatrix} \right),
\end{aligned}
\tag{26}
$$

where the blocks are given by

$$
\begin{aligned}
[\hat{\mathfrak{L}}^{(1)}(\hat{\mathbf{M}})]_{ij} &= \begin{bmatrix} \mu_{ij} & 0 \\ 0 & \mu_{ij} \end{bmatrix}, \\
[\hat{\mathfrak{L}}^{(2)}(\hat{\mathbf{M}})]_{ij} &= \begin{bmatrix} \upsilon_{ij} & 0 \\ 0 & \upsilon_{ij} \end{bmatrix}.
\end{aligned}
\tag{27}
$$

We remark that for the more general case, when the dynamics of each node are given by n differential equations, we need to define n shuffling operators with similar structure to (26). Notice the similarity of structure of the linear, quadratic, and cubic terms in (18). In the next section, we exploit this structure while performing network-based coordinate transformations.

3.2 Linear Modal Transformation

Prior to applying network-based nonlinear transformations, we transform the system to modal coordinates using the linear coordinate transformation

$$\hat{\mathbf{y}} = (\mathbf{T}_N \otimes \mathbf{I}) \, \hat{\mathbf{z}}, \tag{28}$$

where the modal coordinates are defined as $\mathbf{z}_k = [z_k^{(1)} \; z_k^{(2)}]^{\mathrm{T}}$, $\hat{\mathbf{z}} = \mathrm{col}\,[\mathbf{z}_0 \; \ldots \; \mathbf{z}_k \; \ldots$ $\mathbf{z}_{N-1}]$. Moreover, $\mathbf{T}_N = \begin{bmatrix} \mathbf{e}_0 \cdots \mathbf{e}_k \cdots \mathbf{e}_{N-1} \end{bmatrix}$, where $\mathbf{e}_k$ is the k-th eigenvector of the adjacency matrix $\mathbf{A}_N$ corresponding to the k-th modal eigenvalue $\mathrm{e}^{\mathrm{i}\frac{2\pi k}{N}}$, so that $\mathrm{i}^2 = -1$ and $k = 0, \ldots, N-1$. Notice that the mode number $k = 0$ corresponds to a translational symmetry of the system, the mode numbers $k = 1, \ldots, \lfloor \frac{N}{2} \rfloor$ correspond to having k waves along the ring, while the mode numbers $k = \lceil \frac{N}{2} \rceil, \ldots, N-1$ correspond to having $N - k$ waves along the ring (Olson et al. 2014; Orosz et al. 2010). Using the modal coordinates (18) can be written as

$$\dot{\hat{\mathbf{z}}} = \hat{\mathbf{D}}\hat{\mathbf{z}} + \frac{1}{2} \sum_{b=0,1} \sum_{\beta=1,2} \hat{\mathfrak{L}}^{(\beta)}\big(\hat{\mathbf{S}}_b(\hat{\mathbf{z}})\big) \hat{\mathbf{K}}_b^{(\beta)} \hat{\mathbf{z}}$$
$$+ \frac{1}{6} \sum_{b=0,1} \sum_{\beta=1,2} \sum_{d=0,1} \sum_{\delta=1,2} \hat{\mathfrak{L}}^{(\beta)}\big(\hat{\mathbf{S}}_b(\hat{\mathbf{z}})\big) \hat{\mathfrak{L}}^{(\delta)}\big(\hat{\mathbf{S}}_d(\hat{\mathbf{z}})\big) \hat{\mathbf{L}}_{bd}^{(\beta\,\delta)} \hat{\mathbf{z}}. \qquad (29)$$

Here the matrix

$$\hat{\mathbf{D}} = \mathrm{diag}(\mathbf{D}_k), \qquad (30)$$

is block diagonal, and the 2×2 block for mode k is given by

$$\mathbf{D}_k = [\mathfrak{J}_0]^* + [\mathfrak{J}_1]^* \, \mathrm{e}^{\mathrm{i}\frac{2\pi k}{N}}, \qquad (31)$$

for $k = 0, \ldots, N-1$. Note that the block $\mathbf{D}_k$ is in fact the $k+1$-st block along the diagonal due to the presence of modal index 0. The matrices $\hat{\mathbf{S}}_b(\hat{\mathbf{z}}) \in \mathbb{C}^{2N \times 2N}$, $b = 0,\ 1$ in (29) have block structures such that the blocks are given by

$$\mathbf{S}_{0\,k\,\ell}(\mathbf{z}_{f_{k\ell}}) = \begin{bmatrix} z_{f_{k\ell}}^{(1)} & 0 \\ 0 & z_{f_{k\ell}}^{(2)} \end{bmatrix}, \quad \mathbf{S}_{1\,k\,\ell}(\mathbf{z}_{f_{k\ell}}) = \begin{bmatrix} \mathrm{e}^{\mathrm{i}\frac{2\pi(k-\ell)}{N}} z_{f_{k\ell}}^{(1)} & 0 \\ 0 & \mathrm{e}^{\mathrm{i}\frac{2\pi(k-\ell)}{N}} z_{f_{k\ell}}^{(2)} \end{bmatrix}, \qquad (32)$$

where the function

$$f_{k\ell} = \begin{cases} k - \ell & \text{if } k \geq \ell, \\ N + k - \ell & \text{if } k < \ell, \end{cases} \qquad (33)$$

defines the modal indices for the blocks and dictates the cyclic structure of the nonlinear terms.

Since the coefficient matrices in the quadratic and cubic terms of (18) have the same block structure as the Jacobian, they are also diagonalized by the linear modal transformation. The quadratic terms contain the block diagonal matrix

$$\hat{\mathbf{K}}_b^{(\beta)} = \mathrm{diag}(\mathbf{K}_{bk}^{(\beta)}), \qquad (34)$$

with 2×2 blocks

$$\mathbf{K}_{bk}^{(\beta)} = [\partial_b^{(\beta)} \mathfrak{J}_0]^* + [\partial_b^{(\beta)} \mathfrak{J}_1]^* \, \mathrm{e}^{\mathrm{i}\frac{2\pi k}{N}}, \tag{35}$$

for $k = 0, \ldots, N - 1$, while the cubic terms contain the block diagonal matrix

$$\hat{\mathbf{L}}_{bd}^{(\beta \delta)} = \mathrm{diag}(\mathbf{L}_{bdk}^{(\beta \delta)}), \tag{36}$$

with 2×2 blocks

$$\mathbf{L}_{bdk}^{(\beta \delta)} = [\partial_b^{(\beta)} \partial_d^{(\delta)} \mathfrak{J}_0]^* + [\partial_b^{(\beta)} \partial_d^{(\delta)} \mathfrak{J}_1]^* \, \mathrm{e}^{\mathrm{i}\frac{2\pi k}{N}}, \tag{37}$$

for $k = 0, \ldots, N - 1$. The asterisk in (35) and (37) still indicates that the matrices are evaluated at the equilibrium.

The linear coordinate transformation (28) serves two purposes. First, it simplifies the linear analysis of the system: The linear part is decoupled into N pairs of complex differential equations, representing the oscillation modes. Thus, linear stability can be analyzed separately for each mode, and stability is ensured when all the modes are stable. Moreover, the transformation (28) block diagonalizes the nonlinear coefficient matrices in the quadratic and cubic terms [notice the similarity between (30, 31), (34, 35), and (36, 37)], and transforms the matrices $\hat{\mathbf{H}}_0(\hat{\mathbf{y}})$ and $\hat{\mathbf{H}}_1(\hat{\mathbf{y}})$ into modal matrices $\hat{\mathbf{S}}_0(\hat{\mathbf{z}})$ and $\hat{\mathbf{S}}_1(\hat{\mathbf{z}})$, cf. (18, 29). The cyclic structure (33), that appears in both the quadratic and the cubic terms allows us to define nonlinear near-identity transformations for cyclic systems.

3.3 Nonlinear Network-Based Coordinate Transformations

After obtaining the modal coordinates where the linear terms are decoupled, we proceed to simplify the quadratic and cubic terms using network-based transformations. These transformations exploit the structure of the network and allow us to eliminate the second-order and third-order terms for a given mode by solving a small number of algebraic equations. Specifically, for a cyclic system with two equations per node, we need to solve eight coupled algebraic equations to eliminate the quadratic terms for a given mode and 16 coupled equations to eliminate the cubic terms for a given mode. For n equations per mode, these are n^3 and n^4, respectively. For a given mode, we can either eliminate the nonlinear terms up to third order or obtain the normal form if the mode undergoes a bifurcation. We emphasize that this method is independent of the number of nodes N in the system.

3.3.1 Network-Based Quadratic Near-Identity Transformation

To eliminate the quadratic terms in (29), we use the quadratic near-identity transformation

$$\hat{\mathbf{z}} = \big(\hat{\mathbf{I}} + \hat{\mathbf{\Psi}}(\hat{\mathbf{u}})\big)\hat{\mathbf{u}}, \tag{38}$$

where $\hat{\mathbf{u}} = \operatorname{col}[\mathbf{u}_0 \ \ldots \ \mathbf{u}_k \ \ldots \ \mathbf{u}_{N-1}]$ and $\mathbf{u}_k = [u_k^{(1)} u_k^{(2)}]^{\mathrm{T}}$. In $\hat{\boldsymbol{\Psi}}(\hat{\mathbf{u}})$ the 2×2 block corresponding to the mode numbers k, $\ell = 0, \ldots, N-1$ is given by

$$\boldsymbol{\Psi}_{k\ell}(\mathbf{u}_{f_{k\ell}}) = \begin{bmatrix} \overline{\boldsymbol{\psi}}_{k\ell}^{(11)} \cdot \mathbf{u}_{f_{k\ell}} & \overline{\boldsymbol{\psi}}_{k\ell}^{(12)} \cdot \mathbf{u}_{f_{k\ell}} \\ \overline{\boldsymbol{\psi}}_{k\ell}^{(21)} \cdot \mathbf{u}_{f_{k\ell}} & \overline{\boldsymbol{\psi}}_{k\ell}^{(22)} \cdot \mathbf{u}_{f_{k\ell}} \end{bmatrix}, \tag{39}$$

where $\boldsymbol{\psi}_{k\ell}^{(m\,n)} = [\psi_{k\ell}^{(m\,n1)} \ \psi_{k\ell}^{(m\,n2)}]^{\mathrm{T}}$, the bar denotes complex conjugate, $f_{k\ell}$ is given by (33), and the dot stands for the inner product defined as

$$\mathbf{a} \cdot \mathbf{b} = \overline{a}_1 b_1 + \overline{a}_2 b_2. \tag{40}$$

The matrix $\hat{\boldsymbol{\Psi}}(\hat{\mathbf{u}})$ has the same structure as the modal matrices in (32) that appear in the quadratic terms of (29).

In order to derive the coefficients, we obtain $\dot{\hat{\mathbf{z}}}$ in two different ways up to second order. On one hand, we substitute (38) into the right-hand side of (29). On the other hand, we take the time derivative of (38). Comparing these two approaches and considering

$$\dot{\hat{\mathbf{u}}} = \hat{\mathbf{D}}\hat{\mathbf{u}} + \mathscr{O}(\hat{\mathbf{u}}^3), \tag{41}$$

we obtain

$$\left(\hat{\boldsymbol{\Psi}}(\hat{\mathbf{D}}\,\hat{\mathbf{u}}) + \hat{\boldsymbol{\Psi}}(\hat{\mathbf{u}})\,\hat{\mathbf{D}} - \hat{\mathbf{D}}\,\hat{\boldsymbol{\Psi}}(\hat{\mathbf{u}}) \right)\hat{\mathbf{u}} = \frac{1}{2} \left(\sum_{b=0,1} \sum_{\beta=1,2} \hat{\mathfrak{L}}^{(\beta)}\big(\hat{\mathbf{S}}_b(\hat{\mathbf{u}})\big) \hat{\mathbf{K}}_b^{(\beta)} \right)\hat{\mathbf{u}}, \tag{42}$$

where the left-hand side contains the coefficients of the transformation matrix, while the right-hand side contains the quadratic terms we seek to eliminate via the transformation. The similar structure of the matrices on the two sides of (42) allows us to eliminate vector $\hat{\mathbf{u}}$ and comparing the appropriate blocks yields

$$\boldsymbol{\Psi}_{k\ell}(\mathbf{D}_{f_{k\ell}}\mathbf{u}_{f_{k\ell}}) + \boldsymbol{\Psi}_{k\ell}(\mathbf{u}_{f_{k\ell}})\mathbf{D}_\ell - \mathbf{D}_k\boldsymbol{\Psi}_{k\ell}(\mathbf{u}_{f_{k\ell}})$$
$$= \frac{1}{2} \sum_{b=0,1} \sum_{\beta=1,2} \mathfrak{L}^{(\beta)}\big(\mathbf{S}_{bk\ell}(\mathbf{u}_{f_{k\ell}})\big)\mathbf{K}_{b\ell}^{(\beta)}. \tag{43}$$

For each k, ℓ pair this gives a linear system of eight equations with eight unknowns of the form

$$\mathbf{A}_{k\ell}\,\mathbf{b}_{k\ell} = \mathbf{c}_{k\ell}, \tag{44}$$

where the coefficient matrix $\mathbf{A}_{k\ell} \in \mathbb{C}^{8\times8}$ is composed of 2×2 blocks as

$$\mathbf{A}_{k\ell} = \begin{bmatrix} \mathbf{D}_{f_{k\ell}}^{\mathrm{T}} + \xi_{k\ell}^{(11)\,*}\mathbf{I} & \kappa_{\ell 0}^{(21)\,*}\mathbf{I} & -\kappa_{k0}^{(12)\,*}\mathbf{I} & \mathbf{0} \\ \kappa_{\ell 0}^{(12)\,*}\mathbf{I} & \mathbf{D}_{f_{k\ell}}^{\mathrm{T}} + \xi_{k\ell}^{(21)\,*}\mathbf{I} & \mathbf{0} & -\kappa_{k0}^{(12)\,*}\mathbf{I} \\ -\kappa_{k0}^{(21)\,*}\mathbf{I} & \mathbf{0} & \mathbf{D}_{f_{k\ell}}^{\mathrm{T}} + \xi_{k\ell}^{(12)\,*}\mathbf{I} & \kappa_{\ell 0}^{(21)\,*}\mathbf{I} \\ \mathbf{0} & -\kappa_{k0}^{(21)\,*}\mathbf{I} & \kappa_{\ell 0}^{(12)\,*}\mathbf{I} & \mathbf{D}_{f_{k\ell}}^{\mathrm{T}} + \xi_{k\ell}^{(22)\,*}\mathbf{I} \end{bmatrix}. \tag{45}$$

Here we have

$$\kappa_{k\ell}^{(\beta\,\delta)} = \partial_0^{(\delta)} g^{(\beta)} + \partial_1^{(\delta)} g^{(\beta)}\, \mathrm{e}^{\mathrm{i}\frac{2\pi\,(k-\ell)}{N}}, \tag{46}$$

and

$$\xi_{k\ell}^{(\beta\,\delta)\,*} = \kappa_{\ell 0}^{(\beta\,\beta)\,*} - \kappa_{k0}^{(\delta\,\delta)\,*}, \tag{47}$$

for β, $\delta = 1, 2$ where the asterisk indicates that the derivatives are evaluated at the equilibrium. The vector $\mathbf{b}_{k\ell} \in \mathbb{C}^8$ contains the near-identity coefficients defined in (39) that appear on the left-hand side of (43), i.e.,

$$\mathbf{b}_{k\ell} = \left[\psi_{k\ell}^{(111)}\ \psi_{k\ell}^{(112)}\ \psi_{k\ell}^{(121)}\ \psi_{k\ell}^{(122)}\ \psi_{k\ell}^{(211)}\ \psi_{k\ell}^{(212)}\ \psi_{k\ell}^{(221)}\ \psi_{k\ell}^{(222)}\right]^{\mathrm{T}}, \tag{48}$$

while the vector $\mathbf{c}_{k\ell} \in \mathbb{C}^8$ contains the terms that appear on the right-hand side of (43), that is,

$$\mathbf{c}_{k\ell} = \frac{1}{2} \begin{bmatrix} \left[\left(\partial_0^{(1)} + \partial_1^{(1)} \mathrm{e}^{\mathrm{i}\frac{2\pi\ell}{N}}\right)(\kappa_{k\ell}^{(11)})\right]^* \\ \left[\left(\partial_0^{(1)} + \partial_1^{(1)} \mathrm{e}^{\mathrm{i}\frac{2\pi\ell}{N}}\right)(\kappa_{k\ell}^{(12)})\right]^* \\ \left[\left(\partial_0^{(2)} + \partial_1^{(2)} \mathrm{e}^{\mathrm{i}\frac{2\pi\ell}{N}}\right)(\kappa_{k\ell}^{(11)})\right]^* \\ \left[\left(\partial_0^{(2)} + \partial_1^{(2)} \mathrm{e}^{\mathrm{i}\frac{2\pi\ell}{N}}\right)(\kappa_{k\ell}^{(12)})\right]^* \\ \left[\left(\partial_0^{(1)} + \partial_1^{(1)} \mathrm{e}^{\mathrm{i}\frac{2\pi\ell}{N}}\right)(\kappa_{k\ell}^{(21)})\right]^* \\ \left[\left(\partial_0^{(1)} + \partial_1^{(1)} \mathrm{e}^{\mathrm{i}\frac{2\pi\ell}{N}}\right)(\kappa_{k\ell}^{(22)})\right]^* \\ \left[\left(\partial_0^{(2)} + \partial_1^{(2)} \mathrm{e}^{\mathrm{i}\frac{2\pi\ell}{N}}\right)(\kappa_{k\ell}^{(21)})\right]^* \\ \left[\left(\partial_0^{(2)} + \partial_1^{(2)} \mathrm{e}^{\mathrm{i}\frac{2\pi\ell}{N}}\right)(\kappa_{k\ell}^{(22)})\right]^* \end{bmatrix}. \tag{49}$$

We remark that (44) can be solved for each k, ℓ pair separately, that is, when focusing on a chosen mode k, we need to solve N decoupled systems of eight equations. On the other hand, using traditional near-identity transformations would require one to solve $8\,N^2$ coupled equations. Unless a fold bifurcation (or any other resonance) occurs, we shall be able to select the matrix $\hat{\boldsymbol{\Psi}}(\hat{\mathbf{u}})$ so that the dynamics of the system do not contain second-order terms. Using the new coordinates, (41) can be expressed as

$$\dot{\hat{\mathbf{u}}} = \hat{\mathbf{D}}\hat{\mathbf{u}} + \frac{1}{2}\sum_{b=0,1}\sum_{\beta=1,2}\left(\hat{\mathfrak{L}}^{(\beta)}\big(\hat{\mathbf{S}}_b(\hat{\boldsymbol{\Psi}}(\hat{\mathbf{u}})\hat{\mathbf{u}})\big)\hat{\mathbf{K}}_b^{(\beta)} + \hat{\mathfrak{L}}^{(\beta)}\big(\hat{\mathbf{S}}_b(\hat{\mathbf{u}})\big)\hat{\mathbf{K}}_b^{(\beta)}\hat{\boldsymbol{\Psi}}(\hat{\mathbf{u}})\right)\hat{\mathbf{u}}$$

$$+ \frac{1}{6}\sum_{b=0,1}\sum_{\beta=1,2}\sum_{d=0,1}\sum_{\delta=1,2}\hat{\mathfrak{L}}^{(\beta)}\big(\hat{\mathbf{S}}_b(\hat{\mathbf{u}})\big)\hat{\mathfrak{L}}^{(\delta)}\big(\hat{\mathbf{S}}_d(\hat{\mathbf{u}})\big)\hat{\mathbf{L}}_{bd}^{(\beta\,\delta)}\hat{\mathbf{u}}. \tag{50}$$

When comparing (29) and (50), one may notice that while the second-order terms disappear, the transformation generates additional third-order terms. The cubic terms in the bottom row of (50) originate from the cubic terms present in the modal system (29), while the cubic terms in the top row appear due to the quadratic near-identity transformation. It is shown in "Appendix 1" that the two terms appearing in the top row are equal, which yields

$$
\begin{aligned}
\dot{\hat{\mathbf{u}}} =& \hat{\mathbf{D}}\hat{\mathbf{u}} + \sum_{b=0,1}\sum_{\beta=1,2} \hat{\mathfrak{L}}^{(\beta)}\big(\hat{\mathbf{S}}_b(\hat{\mathbf{u}})\big)\hat{\mathbf{K}}_b^{(\beta)}\hat{\boldsymbol{\Psi}}(\hat{\mathbf{u}})\hat{\mathbf{u}} \\
&+ \frac{1}{6}\sum_{b=0,1}\sum_{\beta=1,2}\sum_{d=0,1}\sum_{\delta=1,2} \hat{\mathfrak{L}}^{(\beta)}\big(\hat{\mathbf{S}}_b(\hat{\mathbf{u}})\big)\hat{\mathfrak{L}}^{(\delta)}\big(\hat{\mathbf{S}}_d(\hat{\mathbf{u}})\big)\hat{\mathbf{L}}_{bd}^{(\beta\,\delta)}\hat{\mathbf{u}}.
\end{aligned}
\tag{51}
$$

3.3.2 Network-Based Cubic Near-Identity Transformation

Based on the structure of the cubic terms in (51), we define the cubic near-identity transformation

$$
\hat{\mathbf{u}} = \big(\hat{\mathbf{I}} + \hat{\boldsymbol{\Gamma}}(\hat{\mathbf{w}})\,\hat{\boldsymbol{\Phi}}(\hat{\mathbf{w}})\big)\hat{\mathbf{w}},
\tag{52}
$$

where $\hat{\mathbf{w}} = \mathrm{col}\,[\mathbf{w}_0 \ \ldots \ \mathbf{w}_k \ \ldots \ \mathbf{w}_{N-1}]$ and $\mathbf{w}_k = [w_k^{(1)} \ w_k^{(2)}]^{\mathrm{T}}$. The matrices $\hat{\boldsymbol{\Gamma}}(\hat{\mathbf{w}})$ and $\hat{\boldsymbol{\Phi}}(\hat{\mathbf{w}})$ have a circulant block structure, where the blocks for mode numbers k, $\ell = 0, \ldots, N-1$ are given by

$$
\begin{aligned}
\boldsymbol{\Gamma}_{k\ell}(\mathbf{w}_{f_{k,\ell}}) &= \begin{bmatrix} \overline{\boldsymbol{\gamma}}_{k\ell}^{(11)}\cdot\mathbf{w}_{f_{k\ell}} & \overline{\boldsymbol{\gamma}}_{k\ell}^{(12)}\cdot\mathbf{w}_{f_{k\ell}} \\ \overline{\boldsymbol{\gamma}}_{k\ell}^{(21)}\cdot\mathbf{w}_{f_{k\ell}} & \overline{\boldsymbol{\gamma}}_{k\ell}^{(22)}\cdot\mathbf{w}_{f_{k\ell}} \end{bmatrix}, \\
\boldsymbol{\Phi}_{k\ell}(\mathbf{w}_{f_{k\ell}}) &= \begin{bmatrix} \overline{\boldsymbol{\phi}}_{k\ell}^{(11)}\cdot\mathbf{w}_{f_{k\ell}} & \overline{\boldsymbol{\phi}}_{k\ell}^{(12)}\cdot\mathbf{w}_{f_{k\ell}} \\ \overline{\boldsymbol{\phi}}_{k\ell}^{(21)}\cdot\mathbf{w}_{f_{k\ell}} & \overline{\boldsymbol{\phi}}_{k\ell}^{(22)}\cdot\mathbf{w}_{f_{k\ell}} \end{bmatrix},
\end{aligned}
\tag{53}
$$

where $\boldsymbol{\gamma}_{k\ell}^{(m\,n)} = [\gamma_{k\ell}^{(m\,n1)} \ \gamma_{k\ell}^{(m\,n2)}]^{\mathrm{T}}$ and $\boldsymbol{\phi}_{k\ell}^{(m\,n)} = [\phi_{k\ell}^{(m\,n1)} \ \phi_{k\ell}^{(m\,n2)}]^{\mathrm{T}}$, $f_{k\ell}$ is given by (33), and the inner product is defined by (40).

Again, we may obtain $\dot{\hat{\mathbf{u}}}$ in two ways. On one hand, we may substitute (52) into (51), while on the other hand, we may differentiate (52) with respect to time. Considering

$$
\dot{\hat{\mathbf{w}}} = \hat{\mathbf{D}}\,\hat{\mathbf{w}} + \mathcal{O}(\hat{\mathbf{w}}^4),
\tag{54}
$$

we obtain

$$
\begin{aligned}
&\Big(\hat{\boldsymbol{\Gamma}}(\hat{\mathbf{D}}\hat{\mathbf{w}})\,\hat{\boldsymbol{\Phi}}(\hat{\mathbf{w}}) + \hat{\boldsymbol{\Gamma}}(\hat{\mathbf{w}})\,\hat{\boldsymbol{\Phi}}(\hat{\mathbf{D}}\hat{\mathbf{w}}) + \hat{\boldsymbol{\Gamma}}(\hat{\mathbf{w}})\,\hat{\boldsymbol{\Phi}}(\hat{\mathbf{w}})\hat{\mathbf{D}} - \hat{\mathbf{D}}\hat{\boldsymbol{\Gamma}}(\hat{\mathbf{w}})\hat{\boldsymbol{\Phi}}(\hat{\mathbf{w}})\Big)\hat{\mathbf{w}} \\
&= \Big(\sum_{b=0,1}\sum_{\beta=1,2} \hat{\mathfrak{L}}^{(\beta)}\big(\hat{\mathbf{S}}_b(\hat{\mathbf{w}})\big)\hat{\mathbf{K}}_b^{(\beta)}\hat{\boldsymbol{\Psi}}(\hat{\mathbf{w}}) \\
&\quad + \frac{1}{6}\sum_{b=0,1}\sum_{\beta=1,2}\sum_{d=0,1}\sum_{\delta=1,2} \hat{\mathfrak{L}}^{(\beta)}\big(\hat{\mathbf{S}}_b(\hat{\mathbf{w}})\big)\hat{\mathfrak{L}}^{(\delta)}\big(\hat{\mathbf{S}}_d(\hat{\mathbf{w}})\big)\hat{\mathbf{L}}_{bd}^{(\beta\,\delta)}\Big)\hat{\mathbf{w}}.
\end{aligned}
\tag{55}
$$

where the left-hand side contains the coefficients of the transformation matrices, while the right-hand side contains the cubic terms we seek to eliminate via the transformation. Again, exploiting the similarity of structure of the matrices on the two sides of (55), we can eliminate $\hat{\mathbf{w}}$ and compare the appropriate blocks to get

$$
\begin{aligned}
\sum_{j=0}^{N-1} \bigg(&\boldsymbol{\Gamma}_{kj}(\mathbf{D}_{f_{kj}}\mathbf{w}_{f_{kj}})\boldsymbol{\Phi}_{j\ell}(\mathbf{w}_{f_{j\ell}}) + \boldsymbol{\Gamma}_{kj}(\mathbf{w}_{f_{kj}})\boldsymbol{\Phi}_{j\ell}(\mathbf{D}_{f_{j\ell}}\mathbf{w}_{f_{j\ell}}) \\
&+ \boldsymbol{\Gamma}_{kj}(\mathbf{w}_{f_{kj}})\boldsymbol{\Phi}_{j\ell}(\mathbf{w}_{f_{j\ell}})\mathbf{D}_{\ell} - \mathbf{D}_k \boldsymbol{\Gamma}_{kj}(\mathbf{w}_{f_{kj}})\boldsymbol{\Phi}_{j\ell}(\mathbf{w}_{f_{j\ell}}) \bigg) \\
= \sum_{j=0}^{N-1} \bigg(&\sum_{b=0,1}\sum_{\beta=1,2} \mathcal{L}^{(\beta)}\big(\mathbf{S}_{bkj}(\mathbf{w}_{f_{kj}})\big)\mathbf{K}_{bj}^{(\beta)}\,\boldsymbol{\Psi}_{j\ell}(\mathbf{w}_{f_{j\ell}}) \\
&+ \frac{1}{6}\sum_{b=0,1}\sum_{\beta=1,2}\sum_{d=0,1}\sum_{\delta=1,2} \mathcal{L}^{(\beta)}\big(\mathbf{S}_{bkj}(\mathbf{w}_{f_{kj}})\big)\mathcal{L}^{(\delta)}\big(\mathbf{S}_{dj\ell}(\mathbf{w}_{f_{j\ell}})\big)\mathbf{L}_{bd\ell}^{(\beta\delta)} \bigg),
\end{aligned}
\tag{56}
$$

where the sum over j appears due to the multiplication of circulant matrices.

Each triplet k, j, ℓ yields 16 equations for the products of coefficients $\gamma_{kj}\,\phi_{j\ell}$, (cf. (53)), and 32 different products exist. However, we can combine certain pairs of products (that always occur together) and obtain a set of 16 equations with 16 unknowns for each k, j, ℓ triplet:

$$
\tilde{\mathbf{A}}_{kj\ell}\,\tilde{\mathbf{b}}_{kj\ell} = \tilde{\mathbf{c}}_{kj\ell}.
\tag{57}
$$

The matrix $\tilde{\mathbf{A}}_{kj\ell} \in \mathbb{C}^{16\times 16}$ is composed of four 8×8 blocks such that

$$
\tilde{\mathbf{A}}_{kj\ell} = \begin{bmatrix} \mathbf{E}_{kj\ell} & \mathbf{F}_{kj\ell} \\ \mathbf{G}_{kj\ell} & \mathbf{H}_{kj\ell} \end{bmatrix},
\tag{58}
$$

where

$$
\mathbf{E}_{kj\ell} = \begin{bmatrix}
\mathbf{D}_{f_{j\ell}}^{\mathrm{T}} + \xi_{kj\ell}^{(111)}{}^{*}\mathbf{I} & \kappa_{kj}^{(21)}{}^{*}\mathbf{I} & \kappa_{\ell 0}^{(21)}{}^{*}\mathbf{I} & \mathbf{0} \\
\kappa_{kj}^{(12)}{}^{*}\mathbf{I} & \mathbf{D}_{f_{j\ell}}^{\mathrm{T}} + \xi_{kj\ell}^{(211)}{}^{*}\mathbf{I} & \mathbf{0} & \kappa_{\ell 0}^{(21)}{}^{*}\mathbf{I} \\
\kappa_{\ell 0}^{(12)}{}^{*}\mathbf{I} & \mathbf{0} & \mathbf{D}_{f_{j\ell}}^{\mathrm{T}} + \xi_{kj\ell}^{(121)}{}^{*}\mathbf{I} & \kappa_{kj}^{(21)}{}^{*}\mathbf{I} \\
\mathbf{0} & \kappa_{\ell 0}^{(12)}{}^{*}\mathbf{I} & \kappa_{kj}^{(12)}{}^{*}\mathbf{I} & \mathbf{D}_{f_{j\ell}}^{\mathrm{T}} + \xi_{kj\ell}^{(221)}{}^{*}\mathbf{I}
\end{bmatrix},
$$

$$
\mathbf{F}_{kj\ell} = -\kappa_{k0}^{(12)}{}^{*}\begin{bmatrix} 1 & 0 & 0 & 0 \\ 0 & 1 & 0 & 0 \\ 0 & 0 & 1 & 0 \\ 0 & 0 & 0 & 1 \end{bmatrix} \otimes \mathbf{I}, \quad \mathbf{G}_{kj\ell} = -\kappa_{k0}^{(21)}{}^{*}\begin{bmatrix} 1 & 0 & 0 & 0 \\ 0 & 1 & 0 & 0 \\ 0 & 0 & 1 & 0 \\ 0 & 0 & 0 & 1 \end{bmatrix} \otimes \mathbf{I},
$$

$$\mathbf{H}_{kj\ell} = \begin{bmatrix} \mathbf{D}_{fj\ell}^{\mathrm{T}} + \xi_{kj\ell}^{(112)\,*}\mathbf{I} & \kappa_{kj}^{(21)\,*}\mathbf{I} & \kappa_{\ell 0}^{(21)\,*}\mathbf{I} & \mathbf{0} \\ \kappa_{kj}^{(12)\,*}\mathbf{I} & \mathbf{D}_{fj\ell}^{\mathrm{T}} + \xi_{kj\ell}^{(212)\,*}\mathbf{I} & \mathbf{0} & \kappa_{\ell 0}^{(21)\,*}\mathbf{I} \\ \kappa_{\ell 0}^{(12)\,*}\mathbf{I} & \mathbf{0} & \mathbf{D}_{fj\ell}^{\mathrm{T}} + \xi_{kj\ell}^{(122)\,*}\mathbf{I} & \kappa_{kj}^{(21)\,*}\mathbf{I} \\ \mathbf{0} & \kappa_{\ell 0}^{(12)\,*}\mathbf{I} & \kappa_{kj}^{(12)\,*}\mathbf{I} & \mathbf{D}_{fj\ell}^{\mathrm{T}} + \xi_{kj\ell}^{(222)\,*}\mathbf{I} \end{bmatrix}.$$

$$(59)$$

Here we have

$$\xi_{kj\ell}^{(\beta\,\delta\,\theta)\,*} = \kappa_{kj}^{(\beta\,\beta)\,*} + \kappa_{\ell 0}^{(\delta\,\delta)\,*} - \kappa_{k0}^{(\theta\,\theta)\,*}, \qquad (60)$$

for $\beta,\ \delta,\ \theta = 1, 2$ and $\kappa_{k\ell}^{(\beta\,\delta)}$ is defined in (46). The vector $\tilde{\mathbf{b}}_{kj\ell}$ contains the coefficients defined in (53) that appear on the left-hand side of (56) (see "Appendix 2"), while vector $\tilde{\mathbf{c}}_{kj\ell}$ contains the cubic coefficients that appear on the right-hand side of (56) (see "Appendix 3"). Similar to the quadratic case, (57) can be solved for each k, j, ℓ triplet separately, that is, for a chosen k one need to solve N^2 decoupled systems of 16 equations. Again, using traditional nonlinear near-identity transformations would lead to $16\,N^3$ coupled equations. If there are no bifurcations or resonant third-order terms, (57) can be solved for all triplets k, j, ℓ and all cubic coefficients can be eliminated yielding the form (54).

When bifurcations or resonances occur certain terms cannot be eliminated. However, the set of nonlinear transformations described above allows us to decouple the mode responsible for the bifurcation from the rest of the system. By performing one more linear transformation on this small system, the normal form of the bifurcation can be derived.

4 Network-Based Analysis of the Connected Vehicle System

In this section, we analyze the connected vehicle system (1) using the framework developed above. First, we decompose the connected vehicle network into modes at the linear level and analyze the linear stability of the modes. Then we use nonlinear network-based analysis to eliminate the nonlinearities for the modes responsible for the stability loss. Finally, we investigate the criticality of bifurcations and determine the amplitude of nonlinear oscillations associated with the modal stability loss using normal forms.

Using the vector notation $\mathbf{y}_i = [\widetilde{s}_i \ \ \widetilde{v}_i]^{\mathrm{T}}$, we can rewrite the Taylor approximation (9) into the compact form

$$\dot{\mathbf{y}}_i = [\mathfrak{J}_0]^*\mathbf{y}_i + [\mathfrak{J}_1]^*\mathbf{y}_{i+1} + \frac{1}{2}\sum_{b=0,1}\mathbf{H}_b^{(1)}(\mathbf{y}_{i+b})\left([\partial_b^{(1)}\mathfrak{J}_0]^*\mathbf{y}_i + [\partial_b^{(1)}\mathfrak{J}_1]^*\mathbf{y}_{i+1}\right)$$

$$+ \frac{1}{6}\sum_{b=0,1}\sum_{d=0,1}\mathbf{H}_b^{(1)}(\mathbf{y}_{i+b})\,\mathbf{H}_d^{(1)}(\mathbf{y}_{i+d})\left([\partial_b^{(1)}\partial_d^{(1)}\mathfrak{J}_0]^*\mathbf{y}_i + [\partial_b^{(1)}\partial_d^{(1)}\mathfrak{J}_1]^*\mathbf{y}_{i+1}\right).$$

$$(61)$$

cf. (14). Notice that since only the position coordinates $\widetilde{s}_i$ appear in the nonlinear terms, we do not have to sum for the individual coordinates of $\mathbf{y}_i$. The linear terms in (61) contain the matrices

$$[\mathfrak{J}_0]^* = \begin{bmatrix} 0 & 1 \\ -p & -(\alpha+\beta) \end{bmatrix}, \quad [\mathfrak{J}_1]^* = \begin{bmatrix} 0 & 0 \\ p & \beta \end{bmatrix}, \tag{62}$$

while the coefficient matrices in the quadratic terms are given by

$$[\partial_0^{(1)}\mathfrak{J}_0]^* = -[\partial_0^{(1)}\mathfrak{J}_1]^* = -[\partial_1^{(1)}\mathfrak{J}_0]^* = [\partial_1^{(1)}\mathfrak{J}_1]^* = \begin{bmatrix} 0 & 0 \\ q & 0 \end{bmatrix}, \tag{63}$$

and the cubic terms contain

$$-[\partial_0^{(1)}\partial_0^{(1)}\mathfrak{J}_0]^* = -[\partial_0^{(1)}\partial_1^{(1)}\mathfrak{J}_1]^* = -[\partial_1^{(1)}\partial_1^{(1)}\mathfrak{J}_0]^* = \begin{bmatrix} 0 & 0 \\ r & 0 \end{bmatrix},$$

$$[\partial_0^{(1)}\partial_0^{(1)}\mathfrak{J}_1]^* = [\partial_0^{(1)}\partial_1^{(1)}\mathfrak{J}_0]^* = [\partial_1^{(1)}\partial_1^{(1)}\mathfrak{J}_1]^* = \begin{bmatrix} 0 & 0 \\ r & 0 \end{bmatrix}, \tag{64}$$

where p, q, r are given by (10). For the whole system, (61) can be reformulated as

$$
\begin{aligned}
\dot{\hat{\mathbf{y}}} = &\left(\mathbf{I}_N \otimes [\mathfrak{J}_0]^* + \mathbf{A}_N \otimes [\mathfrak{J}_1]^*\right)\hat{\mathbf{y}} + \frac{1}{2}\sum_{b=0,1} \hat{\mathfrak{L}}^{(1)}\big(\hat{\mathbf{H}}_b(\hat{\mathbf{y}})\big)\left(\mathbf{I}_N \otimes [\partial_b^{(1)}\mathfrak{J}_0]^*\right. \\
&+ \mathbf{A}_N \otimes \left[\partial_b^{(1)}\mathfrak{J}_1]^*\right)\hat{\mathbf{y}} \\
&+ \frac{1}{6}\sum_{b=0,1}\sum_{d=0,1} \hat{\mathfrak{L}}^{(1)}\big(\hat{\mathbf{H}}_b(\hat{\mathbf{y}})\big)\,\hat{\mathfrak{L}}^{(1)}\big(\hat{\mathbf{H}}_d(\hat{\mathbf{y}})\big)\left(\mathbf{I}_N \otimes [\partial_b^{(1)}\partial_d^{(1)}\mathfrak{J}_0]^*\right. \\
&+ \mathbf{A}_N \otimes [\partial_b^{(1)}\partial_d^{(1)}\mathfrak{J}_1]^*\big)\hat{\mathbf{y}},
\end{aligned}
\tag{65}
$$

cf. (18). The linear coordinate transformation (28) yields

$$\dot{\hat{\mathbf{z}}} = \hat{\mathbf{D}}\,\hat{\mathbf{z}} + \frac{1}{2}\sum_{b=0,1} \hat{\mathfrak{L}}^{(1)}\big(\hat{\mathbf{S}}_b(\hat{\mathbf{z}})\big)\,\hat{\mathbf{K}}_b^{(1)}\,\hat{\mathbf{z}} + \frac{1}{6}\sum_{b=0,1}\sum_{d=0,1} \hat{\mathfrak{L}}^{(1)}\big(\hat{\mathbf{S}}_b(\hat{\mathbf{z}})\big)\,\hat{\mathfrak{L}}^{(1)}\big(\hat{\mathbf{S}}_d(\hat{\mathbf{z}})\big)\hat{\mathbf{L}}_{bd}^{(11)}\hat{\mathbf{z}}, \tag{66}$$

cf. (29), where $\hat{\mathbf{D}}$, $\hat{\mathbf{S}}_b(\hat{\mathbf{z}})$, $\hat{\mathbf{K}}_b^{(1)}$, $\hat{\mathbf{L}}_{bd}^{(11)} \in \mathbb{C}^{2N \times 2N}$ are given by (30, 32, 34, 36).

4.1 Linear Stability Analysis

The linear part of (66) consists of N decoupled complex differential equations which represent the linear modes in the system. For the k-th mode, the linear dynamics are given by

$$\begin{bmatrix} \dot{z}_k^{(1)} \\ \dot{z}_k^{(2)} \end{bmatrix} = \begin{bmatrix} 0 & 1 \\ p\,\eta_{k0} & \beta\,\eta_{k0} - \alpha \end{bmatrix} \begin{bmatrix} z_k^{(1)} \\ z_k^{(2)} \end{bmatrix}, \tag{67}$$

where

$$\eta_{k\ell} = \mathrm{e}^{\mathrm{i}\frac{2\pi(k-\ell)}{N}} - 1, \tag{68}$$

for $k, \ell = 0, \ldots, N-1$. Thus, using the trial solution $z_k^{(1)}(t) = z_{k\,0}^{(1)} \mathrm{e}^{\lambda t}$, $z_k^{(2)}(t) = z_{k\,0}^{(2)} \mathrm{e}^{\lambda t}$ with $\lambda, z_{k\,0}^{(1)}, z_{k\,0}^{(2)} \in \mathbb{C}$ the characteristic equation for mode k becomes

$$\lambda^2 + (\alpha + \beta)\,\lambda + p - (\beta\,\lambda + p)\,\mathrm{e}^{\mathrm{i}\frac{2\pi k}{N}} = 0. \tag{69}$$

If both solutions λ have negative real parts, the mode is stable. We remark that when the solutions are complex, they are not complex conjugates, since (67) contains complex coefficients. In fact, mode $N-k$ provides the complex conjugate eigenvalues for mode k. The special mode $k = 0$ gives the eigenvalues $\lambda_{0,1} = 0$ and $\lambda_{0,2} = -\alpha$. The former one corresponds to a translational symmetry of (1) (see Orosz and Stépán 2006), while the latter one stays in the left-half complex plane for $\alpha > 0$. We note that for even N, there is another special mode $k = N/2$ which does not have a complex conjugate mode. The eigenvalues of this mode have negative real parts for $\alpha + 2\beta > 0$.

The critical value of $p = \alpha\,V'(h^*)$, where modes k and $N-k$ lose stability, can be obtained by substituting $\lambda = \mathrm{i}\omega$ into (69), taking the real and imaginary parts, and performing some algebraic manipulation to eliminate ω. This yields

$$p_k = \tfrac{1}{2}(2\beta + \alpha)\Big((2\beta + \alpha)\tan^2\Big(\frac{k\pi}{N}\Big) + \alpha\Big). \tag{70}$$

On the other hand, eliminating p, we may obtain the critical angular frequency

$$\omega_k = (2\beta + \alpha)\tan\Big(\frac{k\pi}{N}\Big), \tag{71}$$

for $k = 1, \ldots, N-1$.

Figure 3 shows how the eigenvalues vary with parameter p for $N = 11$ cars and parameters $\alpha = 1$ [1/s], $\beta = 0$ [1/s]. When p is increased, the eigenvalues move in the complex plane and cross the imaginary axis at p_k with imaginary part ω_k. Here we

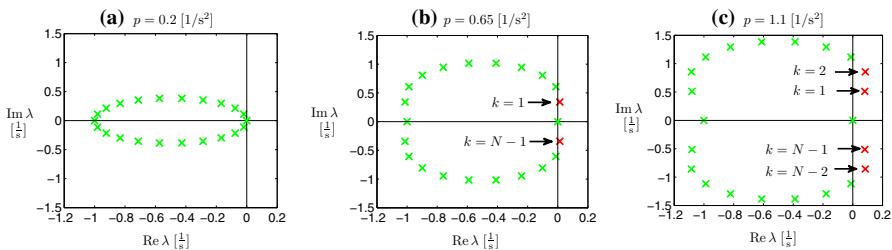**Fig. 3** Eigenvalues in the complex plane for the connected vehicle model (1) when considering $N = 11$ cars and parameters $\alpha = 1$ [1/s], $\beta = 0$ [1/s] and varying the parameter $p = \alpha\,V'(h^*)$. Stable eigenvalues are shown as *green crosses*, while unstable eigenvalues are depicted as *red crosses*. The mode numbers for unstable eigenvalues are indicated in cases (**b**) and (**c**) (Color figure online)

restrict our discussion to $k = 1, \ldots, \lfloor \frac{N}{2} \rfloor$, because for $k = \lceil \frac{N}{2} \rceil, \ldots, N - 1$, we get $p_k = p_{N-k}, \omega_k = -\omega_{N-k}$ due to the complex conjugacy of modes k and $N - k$. Since (70) is monotonically increasing with k when $1 \le k \le \lfloor \frac{N}{2} \rfloor$, the modes lose stability in the increasing order of mode number k. Thus, the uniform flow loses stability when modes 1 (and $N - 1$) lose stability. Since the eigenvalues cross the imaginary axis with a nonzero imaginary part and with finite speed (i.e., $\omega_k > 0$, Re $\frac{d\lambda}{dp}(p_k) > 0$), Hopf bifurcations occur in the corresponding nonlinear system. This leads to nonlinear oscillations with frequency close to (71) and wavelength $(L + N\ell)/k$; see Orosz et al. (2009). The corresponding periodic orbit is embedded in the modal subspace given by modes k and $N - k$. At the linear level, the oscillations can be characterized by the modal coordinates $\mathbf{z}_k$ and $\mathbf{z}_{N-k}$ [see (67)], while at the nonlinear level, further nonlinear transformations are needed to describe the oscillations.

4.2 Near-Identity Transformations

Let us use the network-based nonlinear transformations to eliminate nonlinear terms in (66) at the Hopf point corresponding to the stability loss (i.e., $p = p_1$). This way we can obtain a nonlinear modal equations for modes 1 and $N - 1$ that are decoupled from the rest of the system. To eliminate the quadratic terms in (66), we use the near-identity transformation (38). In this case, (42) simplifies to

$$\left(\hat{\boldsymbol{\Psi}}(\hat{\mathbf{D}}\,\hat{\mathbf{u}}) + \hat{\boldsymbol{\Psi}}(\hat{\mathbf{u}})\,\hat{\mathbf{D}} - \hat{\mathbf{D}}\,\hat{\boldsymbol{\Psi}}(\hat{\mathbf{u}}) \right)\hat{\mathbf{u}} = \frac{1}{2} \Big(\sum_{b=0,1} \hat{\mathfrak{L}}^{(1)} \big(\hat{\mathbf{S}}_b(\hat{\mathbf{u}})\big) \hat{\mathbf{K}}_b^{(1)} \Big)\hat{\mathbf{u}}, \qquad (72)$$

which is equivalent to

$$\boldsymbol{\Psi}_{k\ell}(\mathbf{D}_{f_{k\ell}}\,\mathbf{u}_{f_{k\ell}}) + \boldsymbol{\Psi}_{k\ell}(\mathbf{u}_{f_{k\ell}})\mathbf{D}_\ell - \mathbf{D}_k\boldsymbol{\Psi}_{k\ell}(\mathbf{u}_{f_{k\ell}}) = \frac{1}{2}\sum_{b=0,1}\mathfrak{L}^{(1)}\big(\mathbf{S}_{bk\ell}(\mathbf{u}_{f_{k\ell}})\big)\mathbf{K}_{b\ell}^{(1)}, \;\; (73)$$

cf. (43). Thus, in (44), we have

$$\mathbf{A}_{k\ell} = \begin{bmatrix} \mathbf{D}_{f_{k\ell}}^{\mathrm{T}} & \kappa_{\ell 0}^{(21)*}\mathbf{I} & -\mathbf{I} & \mathbf{0} \\ \mathbf{I} & \mathbf{D}_{f_{k\ell}}^{\mathrm{T}} + \kappa_{\ell 0}^{(22)*}\mathbf{I} & \mathbf{0} & -\mathbf{I} \\ -\kappa_{k0}^{(21)*}\mathbf{I} & \mathbf{0} & \mathbf{D}_{f_{k\ell}}^{\mathrm{T}} - \kappa_{k0}^{(22)*}\mathbf{I} & \kappa_{\ell 0}^{(21)*}\mathbf{I} \\ \mathbf{0} & -\kappa_{k0}^{(21)*}\mathbf{I} & \mathbf{I} & \mathbf{D}_{f_{k\ell}}^{\mathrm{T}} + (\kappa_{\ell 0}^{(22)*} - \kappa_{k0}^{(22)*})\mathbf{I} \end{bmatrix},$$

$$\tag{74}$$

where

$$\kappa_{k\ell}^{(21)*} = p_1\,\eta_{k\ell}, \quad \kappa_{k\ell}^{(22)*} = \beta\,\eta_{k\ell} - \alpha, \tag{75}$$

and $\eta_{k\ell}$ is defined in (68). Note that unlike in (45) here we refrain from using $\xi_{k\ell}^{(\beta\delta)*}$ defined in (47) because $\kappa_{k\ell}^{(11)*} = 0$ for all k, ℓ. Moreover, the right-hand side (49) simplifies to

$$\mathbf{c}_{k\ell} = \mathrm{col}[0\;\;0\;\;0\;\;\frac{q_1}{2}\,\eta_{k\ell}\,\eta_{\ell 0}\;\;0\;\;0\;\;0]^{\mathrm{T}}, \tag{76}$$

where q_1 indicates the value of q at the bifurcation point; cf. (10).

Solving (44) allows us to eliminate all but a few quadratic terms in the $k = 0$ mode in (66). However, as explained above, the $k = 0$ mode does not lose stability and it does not influence the dynamics of the other modes. The equation in the new coordinates becomes

$$
\begin{aligned}
\dot{\hat{\mathbf{u}}} = {}& \hat{\mathbf{D}}\hat{\mathbf{u}} + \frac{1}{2}\hat{\mathbf{R}}(\hat{\mathbf{u}})\hat{\mathbf{u}} + \sum_{b=0,1} \hat{\mathfrak{L}}^{(1)}\big(\hat{\mathbf{S}}_b(\hat{\mathbf{u}})\big)\hat{\mathbf{K}}_b^{(1)}\hat{\boldsymbol{\Psi}}(\hat{\mathbf{u}})\hat{\mathbf{u}} \\
& + \frac{1}{6}\sum_{b=0,1}\sum_{d=0,1}\hat{\mathfrak{L}}^{(1)}\big(\hat{\mathbf{S}}_b(\hat{\mathbf{u}})\big)\hat{\mathfrak{L}}^{(1)}\big(\hat{\mathbf{S}}_d(\hat{\mathbf{u}})\big)\hat{\mathbf{L}}_{bd}^{(11)}\hat{\mathbf{u}},
\end{aligned}
\tag{77}
$$

cf. (51), where the quadratic terms $\hat{\mathbf{R}}(\hat{\mathbf{u}})\hat{\mathbf{u}}$ appear in the $k = 0$ mode, see "Appendix 4".

As our goal is to obtain the nonlinear modal equations for modes 1 and $N - 1$, we proceed by simplifying the cubic terms using the transformation (52) which leads to a simplified form of (55):

$$
\begin{aligned}
& \Big(\hat{\boldsymbol{\Gamma}}(\hat{\mathbf{D}}\hat{\mathbf{w}})\,\hat{\boldsymbol{\Phi}}(\hat{\mathbf{w}}) + \hat{\boldsymbol{\Gamma}}(\hat{\mathbf{w}})\,\hat{\boldsymbol{\Phi}}(\hat{\mathbf{D}}\hat{\mathbf{w}}) + \hat{\boldsymbol{\Gamma}}(\hat{\mathbf{w}})\,\hat{\boldsymbol{\Phi}}(\hat{\mathbf{w}})\hat{\mathbf{D}} - \hat{\mathbf{D}}\hat{\boldsymbol{\Gamma}}(\hat{\mathbf{w}})\hat{\boldsymbol{\Phi}}(\hat{\mathbf{w}})\Big)\hat{\mathbf{w}} \\
& = \Big(\sum_{b=0,1}\hat{\mathfrak{L}}^{(1)}\big(\hat{\mathbf{S}}_b(\hat{\mathbf{w}})\big)\hat{\mathbf{K}}_b^{(1)}\hat{\boldsymbol{\Psi}}(\hat{\mathbf{w}}) + \frac{1}{6}\sum_{b=0,1}\sum_{d=0,1}\hat{\mathfrak{L}}^{(1)}\big(\hat{\mathbf{S}}_b(\hat{\mathbf{w}})\big)\hat{\mathfrak{L}}^{(1)}\big(\hat{\mathbf{S}}_d(\hat{\mathbf{w}})\big)\hat{\mathbf{L}}_{bd}^{(11)}\Big)\hat{\mathbf{w}},
\end{aligned}
\tag{78}
$$

that is equivalent to

$$
\begin{aligned}
\sum_{j=0}^{N-1} \Big(& \boldsymbol{\Gamma}_{kj}(\mathbf{D}_{f_{kj}}\mathbf{w}_{f_{kj}})\boldsymbol{\Phi}_{j\ell}(\mathbf{w}_{f_{j\ell}}) + \boldsymbol{\Gamma}_{kj}(\mathbf{w}_{f_{kj}})\boldsymbol{\Phi}_{j\ell}(\mathbf{D}_{f_{j\ell}}\mathbf{w}_{f_{j\ell}}) \\
& + \boldsymbol{\Gamma}_{kj}(\mathbf{w}_{f_{kj}})\boldsymbol{\Phi}_{j\ell}(\mathbf{w}_{f_{j\ell}})\mathbf{D}_\ell - \mathbf{D}_k\boldsymbol{\Gamma}_{kj}(\mathbf{w}_{f_{kj}})\boldsymbol{\Phi}_{j\ell}(\mathbf{w}_{f_{j\ell}})\Big) \\
& = \sum_{j=0}^{N-1}\Big(\sum_{b=0,1}\mathfrak{L}^{(1)}\big(\mathbf{S}_{bkj}(\mathbf{w}_{f_{kj}})\big)\mathbf{K}_{bj}^{(1)}\,\boldsymbol{\Psi}_{j\ell}(\mathbf{w}_{f_{j\ell}}) \\
& + \frac{1}{6}\sum_{b=0,1}\sum_{d=0,1}\mathfrak{L}^{(1)}\big(\mathbf{S}_{bkj}(\mathbf{w}_{f_{kj}})\big)\mathfrak{L}^{(1)}\big(\mathbf{S}_{dj\ell}(\mathbf{w}_{f_{j\ell}})\big)\mathbf{L}_{bd\ell}^{(11)}\Big),
\end{aligned}
\tag{79}
$$

cf. (56). The matrix $\widetilde{\mathbf{A}}_{kj\ell}$ in (57) has sub-matrices

$$
\mathbf{E}_{kj\ell} = \begin{bmatrix}
\mathbf{D}_{f_{j\ell}}^{\mathrm{T}} & \kappa_{kj}^{(21)*}\mathbf{I} & \kappa_{\ell 0}^{(21)*}\mathbf{I} & \mathbf{0} \\
\mathbf{I} & \mathbf{D}_{f_{j\ell}}^{\mathrm{T}} + \kappa_{kj}^{(22)*}\mathbf{I} & \mathbf{0} & \kappa_{\ell 0}^{(21)*}\mathbf{I} \\
\mathbf{I} & \mathbf{0} & \mathbf{D}_{f_{j\ell}}^{\mathrm{T}} + \kappa_{\ell 0}^{(22)*}\mathbf{I} & \kappa_{kj}^{(21)*}\mathbf{I} \\
\mathbf{0} & \mathbf{I} & \mathbf{I} & \mathbf{D}_{f_{j\ell}}^{\mathrm{T}} + (\kappa_{kj}^{(22)*} + \kappa_{\ell 0}^{(22)*})\mathbf{I}
\end{bmatrix},
$$

$$
\mathbf{F}_{kj\ell} = \begin{bmatrix}
-1 & 0 & 0 & 0 \\
0 & -1 & 0 & 0 \\
0 & 0 & -1 & 0 \\
0 & 0 & 0 & -1
\end{bmatrix} \otimes \mathbf{I}, \quad \mathbf{G}_{kj\ell} = \kappa_{k0}^{(21)*}\mathbf{F}_{kj\ell}, \quad \mathbf{H}_{kj\ell} = \mathbf{E}_{kj\ell} - \kappa_{k0}^{(22)*}\mathbf{I},
\tag{80}
$$

cf. (59), where the $\kappa_{k\ell}^{(21)\,*}$ and $\kappa_{k\ell}^{(22)\,*}$ are given by (75). Finally, the right-hand side (110) (in "Appendix 3") simplifies to

$$\tilde{\mathbf{c}}_{kj\ell} = q_1\,\eta_{kj}\,\eta_{j0}\,[0\ 0\ 0\ 0\ 0\ 0\ 0\ 0\ \psi_{j\ell}^{(111)}\ \ \psi_{j\ell}^{(112)}\ \ 0\ 0\ \psi_{j\ell}^{(121)}\ \ \psi_{j\ell}^{(122)}\ \ 0\ 0]^{\mathrm{T}}$$
$$+ \tfrac{r_1}{6}\,\eta_{kj}\,\eta_{j\ell}\,\eta_{\ell0}\,[0\ 0\ 0\ 0\ 0\ 0\ 0\ 0\ 1\ 0\ 0\ 0\ 0\ 0\ 0\ 0]^{\mathrm{T}}, \qquad (81)$$

where $\eta_{k\ell}$ is given by (68), the $\psi_{j\ell}^{(\cdots)}$ are the solution of (44), while q_1 and r_1 give the values of q and r at the bifurcation point; cf. (10).

When considering the system at the Hopf bifurcation point ($p = p_1$), some cubic terms related to modes $k = 1$ and $k = N - 1$ cannot be eliminated by the nonlinear transformations. In particular, considering (57) the determinant of the matrix $\tilde{\mathbf{A}}_{kj\ell}$ is 0 for the index combinations

$$
\begin{aligned}
&1)\quad k = 1, \quad j = 0, \quad \ell = N - 1,\\
&2)\quad k = 1, \quad j = 0, \quad \ell = 1,\\
&3)\quad k = 1, \quad j = 2, \quad \ell = 1.
\end{aligned}
\qquad (82)
$$

Thus, we obtain that the dynamics of mode 1 are governed by two complex differential equations

$$
\begin{bmatrix} \dot{w}_1^{(1)} \\ \dot{w}_1^{(2)} \end{bmatrix} =
\begin{bmatrix} 0 & 1 \\ \kappa_{10}^{(21)\,*} & \kappa_{10}^{(22)\,*} \end{bmatrix}
\begin{bmatrix} w_1^{(1)} \\ w_1^{(2)} \end{bmatrix} +
\frac{\eta_{10}^2\,\overline{\eta}_{10}\,r_1}{2}
\begin{bmatrix} 0 \\ (w_1^{(1)})^2\,w_{N-1}^{(1)} \end{bmatrix}
$$
$$
+ \overline{\eta}_{10}\,\eta_{20}\,q_1
\begin{bmatrix} 0 \\ \psi_{21}^{(111)}\big(w_1^{(1)}\big)^2\,w_{N-1}^{(1)} + \big(\psi_{21}^{(112)} + \psi_{21}^{(121)}\big)w_1^{(1)}\,w_1^{(2)}\,w_{N-1}^{(1)} + \psi_{21}^{(122)}\big(w_1^{(2)}\big)^2\,w_{N-1}^{(1)} \end{bmatrix},
\tag{83}
$$

where $\eta_{k\ell}$ is defined in (68), while $\kappa_{k\ell}^{(21)\,*}$ and $\kappa_{k\ell}^{(22)\,*}$ are given by (75). The equations for $w_{N-1}^{(1)}$ and $w_{N-1}^{(2)}$ can be obtained by taking the complex conjugate of (83). Explicit expressions for the quadratic near-identity coefficients $\psi_{21}^{(111)}$, $\psi_{21}^{(112)} + \psi_{21}^{(121)}$ and $\psi_{21}^{(122)}$ are given in "Appendix 5". We note that modes 1 and $N - 1$ result in cubic terms in other modes. However, the dynamics for modes $k = 1$ and $k = N - 1$ are not affected by the other modes.

4.3 Bifurcation Analysis

To characterize the nonlinear oscillations in the vicinity of the stability loss, we derive the normal form of the Hopf bifurcation using the nonlinear modal equation (83). Because modes 1 and $N - 1$ contain eigenvalues that cross the imaginary axis at $p = p_1$, the corresponding four-dimensional manifold contains the two-dimensional center manifold. We can obtain the normal form of the Hopf bifurcation by projecting the modal system onto the center manifold. Due to the complex conjugacy of the modes 1 and $N - 1$ involved in the bifurcation, we only need to use one mode to perform the projection and we choose mode 1. At the bifurcation point, mode 1 has one purely imaginary eigenvalue $\lambda_{\mathrm{cr}} = i\omega_1$, where ω_1 is given by (71). Using (75) in the linear part of (83), one may obtain the corresponding eigenvector

$$\mathbf{e} = \begin{bmatrix} 1 \\ \mathrm{i}\,\omega_1 \end{bmatrix}, \tag{84}$$

while left eigenvector corresponding to $\overline{\lambda}_{\mathrm{cr}} = -\mathrm{i}\omega_1$ is given by

$$\mathbf{f} = \frac{1}{\alpha + \omega_1\,\left(2\,\tan(\frac{\pi}{N}) - \mathrm{i}\right)} \begin{bmatrix} \alpha + \omega_1 \tan(\frac{\pi}{N}) \\ 1 + \mathrm{i}\,\tan(\frac{\pi}{N}) \end{bmatrix}. \tag{85}$$

The coefficient in front of the left eigenvector is obtained from the orthogonality condition $\mathbf{f} \cdot \mathbf{e} = 1$, where the inner product is defined by (40).

Let us define the complex variable

$$\zeta = \mathbf{f} \cdot \mathbf{w}_1. \tag{86}$$

Multiplying (83) by $\mathbf{f}$ from the left, we may project the dynamics onto the center manifold; see Kuznetsov (2004). Exploiting $\mathbf{w}_1 \approx \zeta\mathbf{e}$ we obtain the dynamics

$$\dot{\zeta} = \mathrm{i}\omega_1\,\zeta + \delta\,\zeta^2\,\overline{\zeta}, \tag{87}$$

where the cubic coefficient is given by

$$\delta = \frac{\overline{\eta}_{10}\left(1 - \mathrm{i}\tan(\frac{\pi}{N})\right)}{2\left(\alpha + \omega_1\,(2\,\tan(\frac{\pi}{N}) + \mathrm{i})\right)} \left(r_1\,\eta_{10}^2 + 2\,q_1\,\eta_{20}\left(\psi_{21}^{(111)}\right.\right.$$
$$\left.\left. + \mathrm{i}\omega_1\,\left(\psi_{21}^{(112)} + \psi_{21}^{(121)}\right) - \omega_1^2\,\psi_{21}^{(122)}\right)\right). \tag{88}$$

The sign of Re δ determines whether the Hopf bifurcation is supercritical or subcritical. For a supercritical Hopf bifurcation (Re δ < 0), stable oscillations arise around the unstable equilibrium, while in the subcritical case (Re δ > 0), unstable oscillations emerge around the stable equilibrium. Subcritical Hopf bifurcations may lead to bistability as discussed in Orosz et al. (2009). Thus, it is important to determine the criticality of the bifurcation in order to evaluate the effect of the CCC controllers at the nonlinear level.

To calculate the amplitude of the nonlinear oscillations near the Hopf point, we also need the "speed" of the critical eigenvalues crossing the imaginary axis as the parameter p is varied:

$$\mathrm{Re}\,\frac{\mathrm{d}\lambda}{\mathrm{d}p}(p_1) = \frac{\omega_1\,\sin(\frac{2\pi}{N})}{\left(\omega_1\tan(\frac{\pi}{N}) + \alpha\right)^2\cos^4(\frac{\pi}{N}) + 4\,\tan^2(\frac{\pi}{N})\left(\beta(1 + \sin^2(\frac{\pi}{N})) + \alpha\right)^2}. \tag{89}$$

In the vicinity of the Hopf point, the invariant oscillations are well approximated by

$$\zeta(t) \approx \text{Amp}_\zeta \, e^{i(\omega_1 t + \alpha_0)}, \tag{90}$$

where the phase α_0 can be chosen arbitrarily, the frequency ω_1 is given by (71), while the amplitude is given by

$$\text{Amp}_\zeta = \sqrt{-\frac{\text{Re}\,\frac{d\lambda}{dp}(p_1)}{\text{Re}\,\delta}(p - p_1)}. \tag{91}$$

Using (86) the approximations $\mathbf{w}_1 \approx \zeta \mathbf{e}$ and $\mathbf{z}_1 \approx \mathbf{w}_1$ result in

$$\mathbf{z}_1(t) = \begin{bmatrix} z_1^{(1)}(t) \\ z_1^{(2)}(t) \end{bmatrix} \approx \begin{bmatrix} \text{Amp}_\zeta \, e^{i(\omega_1 t + \alpha_0)} \\ \omega_1 \, \text{Amp}_\zeta \, e^{i(\omega_1 t + \frac{\pi}{2} + \alpha_0)} \end{bmatrix}. \tag{92}$$

Finally, using (28) and $\mathbf{y}_i = [\widetilde{s}_i, \widetilde{v}_i]^T$, the velocity of the i-th vehicle can be approximated as

$$\widetilde{v}_i(t) = e^{i\frac{2\pi(i-1)}{N}} z_1^{(2)} + e^{-i\frac{2\pi(i-1)}{N}} z_{N-1}^{(2)} \approx \frac{\text{Amp}_v}{2} \cos(\omega_1 t + \alpha_i), \tag{93}$$

where the peak-to-peak amplitude is given by

$$\text{Amp}_v = 4\,\omega_1 \sqrt{-\frac{\text{Re}\,\frac{d\lambda}{dp}(p_1)}{\text{Re}\,\delta}(p - p_1)}, \tag{94}$$

and $\alpha_i = \alpha_0 + \frac{\pi}{2} + \frac{2\pi}{N}(i-1)$ is the phase offset for the i-th car. Choosing $\alpha_0 = -\frac{\pi}{2} + \frac{2\pi}{N}$ yields $\alpha_i = \frac{2\pi}{N}i$; making it obvious that (93) describes a traveling wave (Orosz and Stépán 2006).

Notice that according to (10), we have $p_1 = \alpha V'(h_{cr}^*)$, that is, when varying the average distance of vehicles h^*, the parameter p changes and the critical value of p_1 corresponds to some critical headway h_{cr}^*. If we wish to consider h^* as the bifurcation parameter, we can use (10) to obtain

$$\text{Re}\,\frac{d\lambda}{dh^*}(h_{cr}^*) = \text{Re}\,\frac{d\lambda}{dp}(p_1)\frac{dp}{dh^*}(h_{cr}^*) = q_1 \,\text{Re}\,\frac{d\lambda}{dp}(p_1), \tag{95}$$

and rewrite the peak-to-peak amplitude for velocity oscillations (94) as

$$\text{Amp}_v = 4\,\omega_1 \sqrt{-q_1 \frac{\text{Re}\,\frac{d\lambda}{dp}(p_1)}{\text{Re}\,\delta}(h^* - h_{cr}^*)}. \tag{96}$$
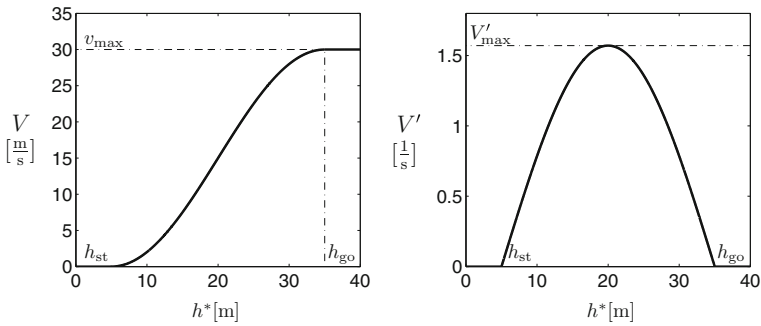
Fig. 4 The nonlinear range policy function (4) (*left*) and its derivative (*right*). The headways h_{st} and h_{go}, the free-flow speed v_{max}, and the maximum of the derivative V'_{max} are indicated. In this case, $h_{st} = 5$ [m], $h_{go} = 35$ [m], $v_{max} = 30$ [m/s], $V'_{max} = \frac{\pi}{2}$ [1/s]

5 Numerical Verification

In this section, we validate our analytical results using numerical continuation for the specific nonlinear function (4); that is plotted together with its derivative in Fig. 4 for $h_{st} = 5$ [m], $h_{go} = 35$ [m], and $v_{max} = 30$ [m/s] yeilding $V'_{max} = \frac{\pi}{2}$ [1/s] that is used in the rest of this section. We chose $h^* = L/N$ as the bifurcation parameter and present the results for different values of the parameters α and β to evaluate the effects of the CCC controller on the system dynamics. Note that due to the properties of the range policy (4), each p_1 corresponds to two h^*_{cr}, values, such that $p > p_1$ holds for the middle range of headways.

5.1 Bifurcation Diagrams

In Fig. 5, the results are summarized in the (h^*, α)-plane for different values of the parameter β when considering $N = 11$ cars. Solid black curves denote the modal stability boundaries, while green dashed curves denote the fold bifurcations of the oscillatory solutions for $k = 1$ (explained further below). In the light gray region, the uniform flow equilibrium is globally stable. In the white region, the equilibrium is unstable and there exist globally stable oscillatory solutions. In the dark gray region, bistability occurs between the stable uniform flow and the oscillations. Since the stability boundaries for modes k and $N - k$ are the same due to complex conjugacy, we only consider $k = 1, \ldots, \lfloor \frac{N}{2} \rfloor$. Each modal boundary encloses a region in the parameter space where the corresponding mode is linearly unstable. Notice that the instability regions for higher mode numbers are contained in the instability regions for lower mode numbers. This corresponds to the fact that (70) increases monotonically with the mode number k between 1 and $\lfloor \frac{N}{2} \rfloor$. Thus, $k = 1$ gives the stability boundary of the uniform flow. Figure 5a shows the two-dimensional bifurcation diagram without relative velocity feedback ($\beta = 0$). In this case, all five modal stability boundaries appear. For $\beta > 0$ the modal stability boundaries become closed curves and the modal
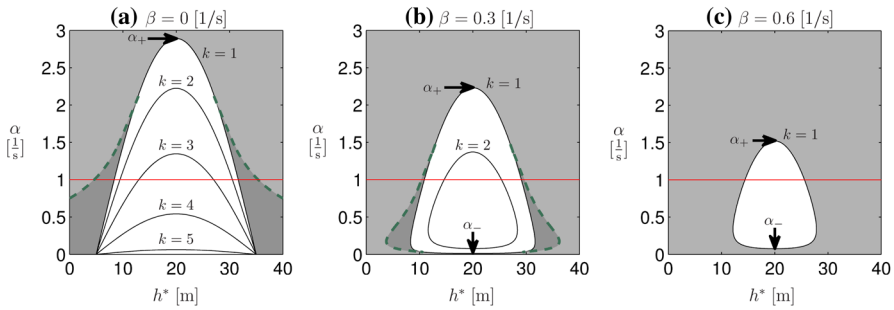
Fig. 5 Two-dimensional bifurcation diagrams in the (h^*, α)-plane for $N = 11$ cars when considering different values of β as indicated. The *black curves* are the linear stability boundaries for the modes $k = 1, \ldots, 5$. The *dashed green curves* show where the periodic solutions for $k = 1$ undergo fold bifurcations. *Light gray shading* indicates globally stable uniform flow. In the *white region*, the uniform flow is unstable and stable oscillations appear. The *dark gray region* corresponds to bistability between the equilibrium and oscillations. The *red horizontal lines* correspond to the panels in Fig. 6 (Color figure online)

instability regions shrink (and may even disappear) when β is increased as depicted in Fig. 5b,c.

In order to quantify how the stability chart changes with β, we determine the maximum α_+ and the minimum α_-; see Fig. 5, and use these extrema to calculate the critical value of β where the linearly unstable domain disappears. To find $\alpha_\pm$, we substitute $V'(h) = V'_{\max}$ and $k = 1$ into (70) which yields

$$\alpha_\pm = (\beta + V'_{\max})\cos^2(\tfrac{\pi}{N}) - 2\beta \pm \sqrt{\left((\beta + V'_{\max})\cos^2(\tfrac{\pi}{N}) - 2\beta\right)^2 - 4\sin^2(\tfrac{\pi}{N})\beta^2}. \tag{97}$$

One can show that α_- increases, while α_+ decreases with β and the instability region disappears when $\alpha_+ = \alpha_-$ that occurs at the β value

$$\beta_{\mathrm{cr}} = V'_{\max} \frac{1 - \sin(\frac{\pi}{N})}{1 + \sin(\frac{\pi}{N})}. \tag{98}$$

That is, for $\beta > \beta_{\mathrm{cr}}$ no unstable region exists. For $N = 11$ cars we obtain $\beta_{\mathrm{cr}} \approx 0.880\,[1/\mathrm{s}]$.

While the linear stability analysis reveals where the uniform traffic flow loses linear stability, the bifurcation analysis gives insight about what happens at the nonlinear level. Here we compare the peak-to-peak amplitude (96) calculated analytically to the amplitudes computed using numerical continuation (Roose and Szalai 2007). In Fig. 6, we plot the branches of oscillations for mode 1 considering different values of β for $N = 11$ cars and $\alpha = 1[1/\mathrm{s}]$; see the red horizontal lines in Fig. 5. The horizontal axis represents the uniform flow equilibrium. Stable and unstable solutions are shown as solid green and dashed red curves, respectively. The oscillatory solutions arise from Hopf bifurcations marked by blue stars and may undergo fold bifurcations marked by black pluses. The zoom-ins at the bottom compare the analytical results (black) and the numerical results (colored) at the vicinity of the Hopf bifurcation points. The bifurcation diagrams are symmetric about $h^* = \frac{h_{\mathrm{go}} + h_{\mathrm{st}}}{2}$ due to the symmetry of the
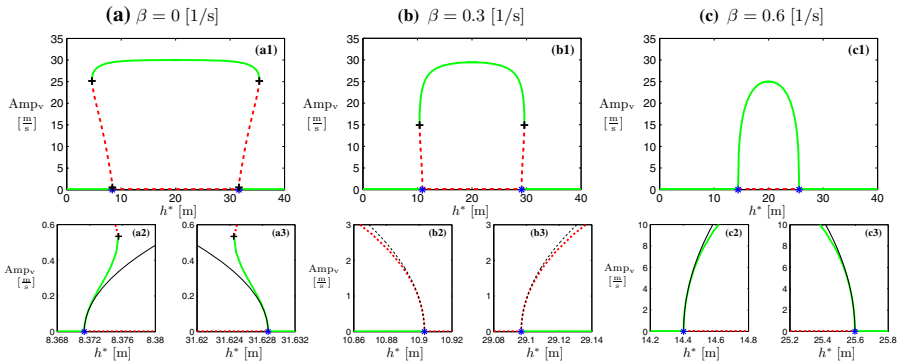
Fig. 6 Bifurcation diagrams for $N = 11$ cars and $\alpha = 1\,[1/s]$ for different values of β as indicated. In *each panel*, the peak-to-peak velocity amplitude Amp_v is shown as a function of the bifurcation parameter h^*. The *horizontal axis* represents the uniform flow equilibrium. Stable states are depicted as *solid green*, and unstable states are shown as *dashed red curves*. Hopf bifurcations are marked by *blue stars*, and fold bifurcations of periodic orbits are marked by *black pluses*. The bottom panels zoom onto the Hopf points and also show the analytical predictions 96 as black lines (Color figure online)

range policy function (4). In each case, the bifurcations partition the diagrams into different regimes of qualitative behavior.

In Fig. 6a, the Hopf bifurcations are supercritical and give rise to stable periodic solutions, but the stability changes via fold bifurcations soon after birth (see the zoomed panels at the bottom). For large amplitudes, the stability of the periodic orbits changes again through fold bifurcations leading to stable large-amplitude oscillations. These bifurcations yield four qualitatively different regimes. For headways outside the high amplitude fold points, the uniform flow is globally stable and no oscillations appear. In the region in between the low-amplitude fold points, the uniform flow is unstable, while the high-amplitude oscillations are globally stable. In the bistable regimes bordered by a high-amplitude fold point and a Hopf point, the uniform flow is linearly stable, but stable large-amplitude oscillations are also present, and the stable states are separated by unstable oscillations. Other bistable regimes are bordered by a Hopf point and a low-amplitude fold point where the uniform flow is unstable, but there exist stable low-amplitude and high-amplitude oscillations separated by unstable oscillations. We remark that this behavior happens in a very narrow parameter domain and is not visible in the two-dimensional bifurcation diagram in Fig. 5a.

When β is increased, the domain where the equilibrium is unstable shrinks as can be observed in Fig. 6b (cf. Fig. 5b). Nonlinear analysis shows that the Hopf bifurcations are now subcritical, leading to unstable oscillations. The low-amplitude fold bifurcations disappear while the high amplitude fold points move closer to each other. Here the bifurcations create three regimes of qualitatively different behavior. Again outside the fold points, the uniform flow is globally stable, while between the Hopf points, the uniform flow is unstable and the high-amplitude velocity oscillations are globally stable. However, only one kind of bistable regime exists between the
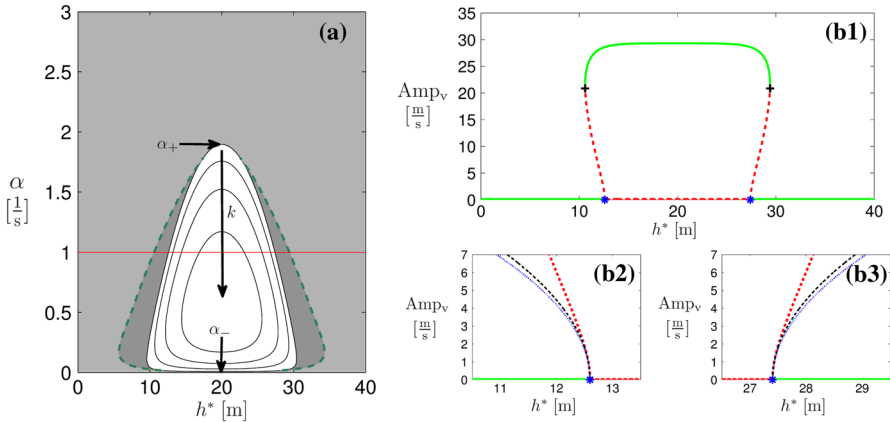
Fig. 7 **a** Two-dimensional bifurcation diagram for $N = 33$ cars and $\beta = 0.6\,[1/s]$. **b** Bifurcation diagram for $N = 33$ cars, $\alpha = 1\,[1/s]$, and $\beta = 0.6\,[1/s]$. The same notation is used as in Figs. 5 and 6. The *blue dotted curves* in panels (*b2*) and (*b3*) show the analytical prediction for $N \to \infty$ as given by (102) (Color figure online)

Hopf and fold points, where the equilibrium and the large-amplitude oscillations are both stable. For larger β values, stable oscillatory solutions exist only between the Hopf points where the uniform flow is unstable as shown in Fig. 6c and outside this regime, the uniform flow is globally stable. When β is increased even further, the Hopf points move closer to each other and the branch of stable oscillations disappears at $\beta \approx 0.786\,[1/s]$.

5.2 Large N Limit

Now we demonstrate how the number of cars N influences the nonlinear behavior. Indeed, we are interested in the large N limit. First, we consider $N = 33$ cars and $\beta = 0.6\,[1/s]$. Figure 7a shows a two-dimensional bifurcation diagram in the (h^*, α)-plane (cf. Fig. 5b), while a bifurcation diagram is displayed in Fig. 7b for $\alpha = 1\,[1/s]$, (cf. Fig. 6b). The linearly unstable region is similar to the 11-car case, but we have larger number of modal stability boundaries. Still mode 1 determines the linear stability of the uniform flow. One may observe that stability is lost via subcritical Hopf bifurcations, and the bifurcation diagram is qualitatively similar to the one in Fig. 6b.

To get a broader picture about how the nonlinear oscillatory solutions depend on the number of vehicles, we consider $\alpha = 1\,[1/s]$ and evaluate the sign of $\mathrm{Re}\,\delta$ in (87) while varying N and β. We plot the results in Fig. 8, where supercritical Hopf bifurcations occur in the green area, subcritical Hopf bifurcations occur in the red area, and no bifurcations take place in the white area. The black curve denotes the linear stability boundary, while the blue curve denotes the boundary where criticality of the Hopf bifurcation changes. For a small numbers of cars ($N < 10$), only supercritical Hopf bifurcations are possible. When N is increased, the unstable regime
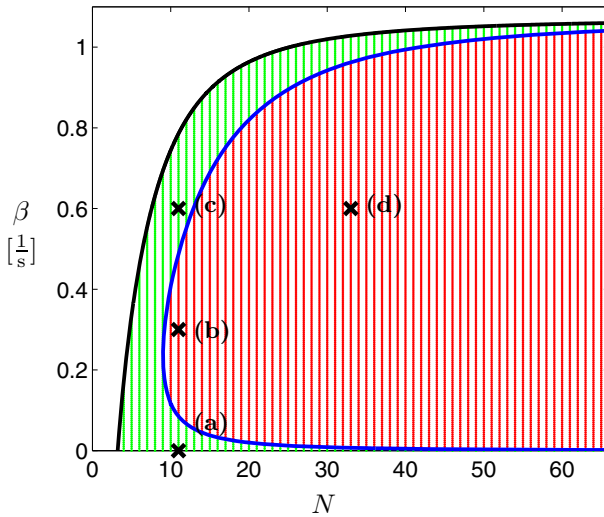
Fig. 8 Criticality diagram for $\alpha = 1\,[1/\mathrm{s}]$. *Green shading* represents supercritical Hopf bifurcations, *red shading* represents subcritical Hopf bifurcations. These are separated by the *blue curve*. The system does not undergo a Hopf bifurcation in the white region and the Hopf boundary is represented by the *black curve*. The points marked (*a*), (*b*), (*c*) correspond to the three cases examined in Figs. 5 and 6, while the point marked (*d*) corresponds to Fig. 7 (Color figure online)

expands and the bifurcation turns subcritical for a range of β that also grows with N.

In the large N limit, the black stability boundary approaches an asymptotic value that can be obtained by using $p_1 = \alpha V'_{\max}$ and $N \to \infty$ in (70):

$$\beta_{\max} = V'_{\max} - \frac{\alpha}{2}. \tag{99}$$

Considering the range policy (4) and $\alpha = 1\,[1/\mathrm{s}]$ yields $\beta_{\max} = (\pi - 1)/2 \approx 1.071\,[1/\mathrm{s}]$; see the black curve in Fig. 8. Also, the blue criticality boundary approaches the horizontal axis and the black Hopf bifurcation boundary which indicates that the typical behavior is subcritical for large number of cars as demonstrated in Fig. 7. This can also be seen when replacing the trigonometric functions in (88) by their Taylor series which in the large N limit yields

$$\operatorname{Re}\delta_\infty \approx \frac{3\,q_1^2\,\beta}{(3\beta + \alpha)^2\alpha^2}\left(\frac{2\pi}{N}\right)^2 > 0, \tag{100}$$

showing that $\operatorname{Re}\delta_\infty$ is positive for the whole domain $0 < \beta < \beta_{\max}$.

Similarly, taking the large N limit in (89) gives

$$\operatorname{Re}\frac{\mathrm{d}\lambda}{\mathrm{d}h^*}(h^*_{\mathrm{cr}\,\infty}) \approx \frac{q_1(2\beta + \alpha)}{2\,\alpha^2}\left(\frac{2\pi}{N}\right)^2. \tag{101}$$

Thus, for large N, the Hopf amplitude (96) is given by

$$\text{Amp}_{v\,\infty} \approx 4(3\beta + \alpha)(2\beta + \alpha)\frac{\pi}{N}\sqrt{-\frac{2\beta + \alpha}{6\beta\,q_1}(h^* - h_{\text{cr}}^*)}, \qquad (102)$$

where we used (71) with $k = 1$. The blue dotted curves in Fig. 7 correspond to (102), and these are well approximated by the black curves shown for $N = 33$. However, observe that $\text{Amp}_{v\,\infty} \to \infty$ as $\beta \to 0$ or $q_1 \to 0$. The latter case corresponds to $\beta \to \beta_{\max}$, since the black stability boundary in Fig. 8 corresponds to the inflection point of the range policy. This shows that in the large N limit, the lower criticality boundary tends to $\beta = 0$, while the upper criticality boundary tends to $\beta = \beta_{\max}$. Thus, choosing sufficiently large β guarantees global stability of the uniform flow, which demonstrates the benefit of relative velocity feedback in CCC design.

6 Conclusion

In this paper, we analyzed the dynamics of connected vehicle systems where vehicles execute nonlinear connected cruise control (CCC) while responding to signals received from other vehicles ahead. These systems were used as a motivation to develop network-based bifurcation analysis based on nonlinear normal modes (NNMs). Our method simplified the bifurcation analysis of large coupled systems with cyclic symmetry. A linear transformation was used to write the dynamics into modal coordinates, and subsequent nonlinear network-based transformations were used to eliminate the quadratic and cubic terms. These led to a small number of algebraic equations for each mode that can be solved without considering the dynamics of other modes.

We applied the algorithm to a connected vehicle system where each vehicle reacts to the distance and the relative velocity to the vehicle directly ahead. After performing the linear transformation, we detected the mode responsible for the stability loss of the uniform flow. We then decoupled this mode from the rest of the system using the nonlinear near-identity transformations and projected the dynamics onto the center manifold to find the normal form of the Hopf bifurcation. This allowed us to analytically determine the criticality and amplitudes the nonlinear oscillations arising at the bifurcation point and observe the effects of the CCC feedback law on the system dynamics. We validated our network-based algorithm by comparing the analytical results to those obtained by numerical continuation.

Because we found the network-based algorithm to be effective in analyzing the dynamics of the connected vehicle system with simple structure, we seek to extend this algorithm to more realistic scenarios. Future work includes generalizing the algorithm to systems with more complicated communication structures where vehicles may respond to multiple cars ahead and to nonhomogenous systems where different vehicles have different control parameters and communication strategies. We are also planning to analyze the effect of time

delays arising in the V2V communication due to intermittencies and packet drops (Qin et al. 2014).

Appendix 1: Simplification of Cubic Terms

Before applying the cubic near-identity transformation (52), we need to express all the cubic terms of (50) using multiples of two circulant matrices. However, the cubic term $\hat{\mathfrak{L}}^{(\beta)}\left(\hat{\mathbf{S}}_b\left(\hat{\boldsymbol{\Psi}}(\hat{\mathbf{u}})\hat{\mathbf{u}}\right)\right)\hat{\mathbf{K}}_b^{(\beta)}\hat{\mathbf{u}}$ does not appear to have such structure. By spelling out the components corresponding to the dynamics of mode k (in other words the $k+1$-st row pair), we obtain

$$
\left[\sum_{b=0,1}\sum_{\beta=1,2}\hat{\mathfrak{L}}^{(\beta)}(\hat{\mathbf{S}}_b(\hat{\boldsymbol{\Psi}}(\hat{\mathbf{u}})\hat{\mathbf{u}}))\hat{\mathbf{K}}_b^{(\beta)}\hat{\mathbf{u}}\right]_k
$$
$$
=\sum_{j=0}^{N-1}\sum_{\ell=0}^{N-1}\sum_{b=0,1}\sum_{\beta=1,2}\sum_{\delta=1,2}\begin{bmatrix}\mathrm{e}^{\mathrm{i}\frac{2\pi b(k-\ell)}{N}}\left[\partial_b^{(\beta)}\kappa_{\ell 0}^{(1\delta)}\right]^*\left(\overline{\boldsymbol{\psi}}_{m(\ell)\,j}^{(\beta 1)}\cdot\mathbf{u}_{f_{m(\ell)}\,j}\,u_j^{(1)}+\overline{\boldsymbol{\psi}}_{m(\ell)\,j}^{(\beta 2)}\cdot\mathbf{u}_{f_{m(\ell)}\,j}\,u_j^{(2)}\right)u_\ell^{(\delta)}\\[2mm]\mathrm{e}^{\mathrm{i}\frac{2\pi b(k-\ell)}{N}}\left[\partial_b^{(\beta)}\kappa_{\ell 0}^{(2\delta)}\right]^*\left(\overline{\boldsymbol{\psi}}_{m(\ell)\,j}^{(\beta 1)}\cdot\mathbf{u}_{f_{m(\ell)}\,j}\,u_j^{(1)}+\overline{\boldsymbol{\psi}}_{m(\ell)\,j}^{(\beta 2)}\cdot\mathbf{u}_{f_{m(\ell)}\,j}\,u_j^{(2)}\right)u_\ell^{(\delta)}\end{bmatrix},
$$
(103)

where $m(\ell)$ is given as

$$
m(\ell)=f_{k\ell}=\begin{cases}k-\ell & \text{if }\ k\geq\ell,\\ N+k-\ell & \text{if }\ k<\ell.\end{cases}
$$
(104)

If we consider a change of indexes $\sigma=f_{k\ell}$, we get

$$
\left[\sum_{b=0,1}\hat{\mathfrak{L}}^{(\beta)}(\hat{\mathbf{S}}_b(\hat{\boldsymbol{\Psi}}(\hat{\mathbf{u}})\hat{\mathbf{u}}))\hat{\mathbf{K}}_b^{(\beta)}\hat{\mathbf{u}}\right]_k
$$
$$
=\sum_{j=0}^{N-1}\sum_{\sigma=0}^{N-1}\sum_{b=0,1}\sum_{\beta=1,2}\sum_{\delta=1,2}\begin{bmatrix}\mathrm{e}^{\mathrm{i}\frac{2\pi b\sigma}{N}}\left[\partial_b^{(\beta)}\kappa_{f_{k\sigma}0}^{(1\delta)}\right]^*\left(\overline{\boldsymbol{\psi}}_{\sigma\,j}^{(\beta 1)}\cdot\mathbf{u}_{f_\sigma\,j}\,u_j^{(1)}+\overline{\boldsymbol{\psi}}_{\sigma\,j}^{(\beta 2)}\cdot\mathbf{u}_{f_\sigma\,j}\,u_j^{(2)}\right)u_{f_{k\sigma}}^{(\delta)}\\[2mm]\mathrm{e}^{\mathrm{i}\frac{2\pi b\sigma}{N}}\left[\partial_b^{(\beta)}\kappa_{f_{k\sigma}0}^{(2\delta)}\right]^*\left(\overline{\boldsymbol{\psi}}_{\sigma\,j}^{(\beta 1)}\cdot\mathbf{u}_{f_\sigma\,j}\,u_j^{(1)}+\overline{\boldsymbol{\psi}}_{\sigma\,j}^{(\beta 2)}\cdot\mathbf{u}_{f_\sigma\,j}\,u_j^{(2)}\right)u_{f_{k\sigma}}^{(\delta)}\end{bmatrix}.
$$
(105)

Similarly, the k-th modal component of $\hat{\mathfrak{L}}^{(\beta)}\left(\hat{\mathbf{S}}_b(\hat{\mathbf{u}})\right)\hat{\mathbf{K}}_b^{(\beta)}\hat{\boldsymbol{\Psi}}(\hat{\mathbf{u}})\hat{\mathbf{u}}$ can be expanded as

$$
\left[\sum_{b=0,1}\sum_{\beta=1,2}\hat{\mathfrak{L}}^{(\beta)}(\hat{\mathbf{S}}_b(\hat{\mathbf{u}}))\hat{\mathbf{K}}_b^{(\beta)}\hat{\boldsymbol{\Psi}}(\hat{\mathbf{u}})\hat{\mathbf{u}}\right]_k
$$
$$
=\sum_{j=0}^{N-1}\sum_{\ell=0}^{N-1}\sum_{b=0,1}\sum_{\delta=1,2}\sum_{\beta=1,2}\begin{bmatrix}\mathrm{e}^{\mathrm{i}\frac{2\pi b(k-\ell)}{N}}\left[\partial_b^{(\beta)}\kappa_{\ell 0}^{(1\delta)}\right]^*\left(\overline{\boldsymbol{\psi}}_{\ell\,j}^{(\delta 1)}\cdot\mathbf{u}_{f_\ell\,j}\,u_j^{(1)}+\overline{\boldsymbol{\psi}}_{\ell\,j}^{(\delta 2)}\cdot\mathbf{u}_{f_\ell\,j}\,u_j^{(2)}\right)u_j^{(\beta)}\\[2mm]\mathrm{e}^{\mathrm{i}\frac{2\pi b(k-\ell)}{N}}\left[\partial_b^{(\beta)}\kappa_{\ell 0}^{(2\delta)}\right]^*\left(\overline{\boldsymbol{\psi}}_{\ell\,j}^{(\delta 1)}\cdot\mathbf{u}_{f_\ell\,j}\,u_j^{(1)}+\overline{\boldsymbol{\psi}}_{\ell\,j}^{(\delta 2)}\cdot\mathbf{u}_{f_\ell\,j}\,u_j^{(2)}\right)u_{f_{k\ell}}^{(\beta)}\end{bmatrix}.
$$
(106)

If we re-label the δ and β, we obtain

$$
\left[\sum_{b=0,1}\sum_{\beta=1,2}\hat{\mathfrak{L}}^{(\beta)}(\hat{\mathbf{S}}_b(\hat{\mathbf{u}}))\hat{\mathbf{K}}_b^{(\beta)}\hat{\boldsymbol{\Psi}}(\hat{\mathbf{u}})\hat{\mathbf{u}}\right]_k
$$

$$
=\sum_{j=0}^{N-1}\sum_{\ell=0}^{N-1}\sum_{b=0,1}\sum_{\beta=1,2}\sum_{\delta=1,2}\left[\begin{array}{c}\mathrm{e}^{\mathrm{i}\frac{2\pi b(k-\ell)}{N}}\left[\partial_b^{(\delta)}\kappa_{\ell 0}^{(1\beta)}\right]^*\left(\overline{\boldsymbol{\psi}}_{\ell j}^{(\beta 1)}\cdot\mathbf{u}_{f_\ell j}\,u_j^{(1)}+\overline{\boldsymbol{\psi}}_{\ell j}^{(\beta 2)}\cdot\mathbf{u}_{f_\ell j}\,u_j^{(2)}\right)u_{f k\ell}^{(\delta)}\\\mathrm{e}^{\mathrm{i}\frac{2\pi b(k-\ell)}{N}}\left[\partial_b^{(\delta)}\kappa_{\ell 0}^{(2\beta)}\right]^*\left(\overline{\boldsymbol{\psi}}_{\ell j}^{(\beta 1)}\cdot\mathbf{u}_{f_\ell j}\,u_j^{(1)}+\overline{\boldsymbol{\psi}}_{\ell j}^{(\beta 2)}\cdot\mathbf{u}_{f_\ell j}\,u_j^{(2)}\right)u_{f k\ell}^{(\delta)}\end{array}\right].
$$

$$(107)$$

Considering (105) and (107) for the same values of j, β, and δ, and for $\sigma=\ell$, we can show that

$$
\sum_{b=0,1}\mathrm{e}^{\mathrm{i}\frac{2\pi b\sigma}{N}}\left[\partial_b^{(\beta)}\kappa_{f k\sigma 0}^{(1\delta)}\right]^*=\sum_{b=0,1}\mathrm{e}^{\mathrm{i}\frac{2\pi b(k-\ell)}{N}}\left[\partial_b^{(\delta)}\kappa_{\ell 0}^{(1\beta)}\right]^*,
\tag{108}
$$

and hence (105) and (107) are equal. This means that (50) and (51) are identical.

Appendix 2: Cubic Near-Identity Coefficients (Left Hand Side)

The coefficient vector $\tilde{\mathbf{b}}_{kj\ell}$ in (57) is given by

$$
\tilde{\mathbf{b}}_{kj\ell}=\begin{bmatrix}
\gamma_{kj}^{(111)}\phi_{j\ell}^{(111)}+\gamma_{kj}^{(121)}\phi_{j\ell}^{(211)}\\
\gamma_{kj}^{(111)}\phi_{j\ell}^{(112)}+\gamma_{kj}^{(121)}\phi_{j\ell}^{(212)}\\
\gamma_{kj}^{(112)}\phi_{j\ell}^{(111)}+\gamma_{kj}^{(122)}\phi_{j\ell}^{(211)}\\
\gamma_{kj}^{(112)}\phi_{j\ell}^{(112)}+\gamma_{kj}^{(122)}\phi_{j\ell}^{(212)}\\
\gamma_{kj}^{(111)}\phi_{j\ell}^{(121)}+\gamma_{kj}^{(121)}\phi_{j\ell}^{(221)}\\
\gamma_{kj}^{(111)}\phi_{j\ell}^{(122)}+\gamma_{kj}^{(121)}\phi_{j\ell}^{(222)}\\
\gamma_{kj}^{(112)}\phi_{j\ell}^{(121)}+\gamma_{kj}^{(122)}\phi_{j\ell}^{(221)}\\
\gamma_{kj}^{(112)}\phi_{j\ell}^{(122)}+\gamma_{kj}^{(122)}\phi_{j\ell}^{(222)}\\
\gamma_{kj}^{(211)}\phi_{j\ell}^{(111)}+\gamma_{kj}^{(221)}\phi_{j\ell}^{(211)}\\
\gamma_{kj}^{(211)}\phi_{j\ell}^{(112)}+\gamma_{kj}^{(221)}\phi_{j\ell}^{(212)}\\
\gamma_{kj}^{(212)}\phi_{j\ell}^{(111)}+\gamma_{kj}^{(222)}\phi_{j\ell}^{(211)}\\
\gamma_{kj}^{(212)}\phi_{j\ell}^{(112)}+\gamma_{kj}^{(222)}\phi_{j\ell}^{(212)}\\
\gamma_{kj}^{(211)}\phi_{j\ell}^{(121)}+\gamma_{kj}^{(221)}\phi_{j\ell}^{(221)}\\
\gamma_{kj}^{(211)}\phi_{j\ell}^{(122)}+\gamma_{kj}^{(221)}\phi_{j\ell}^{(222)}\\
\gamma_{kj}^{(212)}\phi_{j\ell}^{(121)}+\gamma_{kj}^{(222)}\phi_{j\ell}^{(221)}\\
\gamma_{kj}^{(212)}\phi_{j\ell}^{(122)}+\gamma_{kj}^{(222)}\phi_{j\ell}^{(222)}
\end{bmatrix},
\tag{109}
$$

where the constants $\gamma_{kj}^{(\cdots)}$ and $\phi_{j\ell}^{(\cdots)}$ are defined in (53).

Appendix 3: Cubic Near-Identity Coefficients (Right Hand Side)

The coefficient vector $\tilde{\mathbf{c}}_{kj\ell}$ in (57) is given by

$$
\tilde{\mathbf{c}}_{kj\ell} =
\begin{bmatrix}
\left(\sum_{\beta=1,2}\psi_{j\ell}^{(\beta 11)}(\partial_0^{(\beta)}+\mathrm{e}^{\mathrm{i}\frac{2\pi\,(j)}{N}}\partial_1^{(\beta)})\right)\kappa_{kj}^{(11)\,*} \\[4pt]
\left(\sum_{\beta=1,2}\psi_{j\ell}^{(\beta 12)}(\partial_0^{(\beta)}+\mathrm{e}^{\mathrm{i}\frac{2\pi\,(j)}{N}}\partial_1^{(\beta)})\right)\kappa_{kj}^{(11)\,*} \\[4pt]
\left(\sum_{\beta=1,2}\psi_{j\ell}^{(\beta 11)}(\partial_0^{(\beta)}+\mathrm{e}^{\mathrm{i}\frac{2\pi\,(j)}{N}}\partial_1^{(\beta)})\right)\kappa_{kj}^{(12)\,*} \\[4pt]
\left(\sum_{\beta=1,2}\psi_{j\ell}^{(\beta 12)}(\partial_0^{(\beta)}+\mathrm{e}^{\mathrm{i}\frac{2\pi\,(j)}{N}}\partial_1^{(\beta)})\right)\kappa_{kj}^{(12)\,*} \\[4pt]
\left(\sum_{\beta=1,2}\psi_{j\ell}^{(\beta 21)}(\partial_0^{(\beta)}+\mathrm{e}^{\mathrm{i}\frac{2\pi\,(j)}{N}}\partial_1^{(\beta)})\right)\kappa_{kj}^{(11)\,*} \\[4pt]
\left(\sum_{\beta=1,2}\psi_{j\ell}^{(\beta 22)}(\partial_0^{(\beta)}+\mathrm{e}^{\mathrm{i}\frac{2\pi\,(j)}{N}}\partial_1^{(\beta)})\right)\kappa_{kj}^{(11)\,*} \\[4pt]
\left(\sum_{\beta=1,2}\psi_{j\ell}^{(\beta 21)}(\partial_0^{(\beta)}+\mathrm{e}^{\mathrm{i}\frac{2\pi\,(j)}{N}}\partial_1^{(\beta)})\right)\kappa_{kj}^{(12)\,*} \\[4pt]
\left(\sum_{\beta=1,2}\psi_{j\ell}^{(\beta 22)}(\partial_0^{(\beta)}+\mathrm{e}^{\mathrm{i}\frac{2\pi\,(j)}{N}}\partial_1^{(\beta)})\right)\kappa_{kj}^{(12)\,*} \\[4pt]
\left(\sum_{\beta=1,2}\psi_{j\ell}^{(\beta 11)}(\partial_0^{(\beta)}+\mathrm{e}^{\mathrm{i}\frac{2\pi\,(j)}{N}}\partial_1^{(\beta)})\right)\kappa_{kj}^{(21)\,*} \\[4pt]
\left(\sum_{\beta=1,2}\psi_{j\ell}^{(\beta 12)}(\partial_0^{(\beta)}+\mathrm{e}^{\mathrm{i}\frac{2\pi\,(j)}{N}}\partial_1^{(\beta)})\right)\kappa_{kj}^{(21)\,*} \\[4pt]
\left(\sum_{\beta=1,2}\psi_{j\ell}^{(\beta 11)}(\partial_0^{(\beta)}+\mathrm{e}^{\mathrm{i}\frac{2\pi\,(j)}{N}}\partial_1^{(\beta)})\right)\kappa_{kj}^{(22)\,*} \\[4pt]
\left(\sum_{\beta=1,2}\psi_{j\ell}^{(\beta 12)}(\partial_0^{(\beta)}+\mathrm{e}^{\mathrm{i}\frac{2\pi\,(j)}{N}}\partial_1^{(\beta)})\right)\kappa_{kj}^{(22)\,*} \\[4pt]
\left(\sum_{\beta=1,2}\psi_{j\ell}^{(\beta 21)}(\partial_0^{(\beta)}+\mathrm{e}^{\mathrm{i}\frac{2\pi\,(j)}{N}}\partial_1^{(\beta)})\right)\kappa_{kj}^{(21)\,*} \\[4pt]
\left(\sum_{\beta=1,2}\psi_{j\ell}^{(\beta 22)}(\partial_0^{(\beta)}+\mathrm{e}^{\mathrm{i}\frac{2\pi\,(j)}{N}}\partial_1^{(\beta)})\right)\kappa_{kj}^{(21)\,*} \\[4pt]
\left(\sum_{\beta=1,2}\psi_{j\ell}^{(\beta 21)}(\partial_0^{(\beta)}+\mathrm{e}^{\mathrm{i}\frac{2\pi\,(j)}{N}}\partial_1^{(\beta)})\right)\kappa_{kj}^{(22)\,*} \\[4pt]
\left(\sum_{\beta=1,2}\psi_{j\ell}^{(\beta 22)}(\partial_0^{(\beta)}+\mathrm{e}^{\mathrm{i}\frac{2\pi\,(j)}{N}}\partial_1^{(\beta)})\right)\kappa_{kj}^{(22)\,*}
\end{bmatrix}
$$

$$
+\ \frac{1}{6}
\begin{bmatrix}
(\partial_0^{(1)}+\mathrm{e}^{\mathrm{i}\frac{2\pi\,(k-j)}{N}}\partial_1^{(1)})(\partial_0^{(1)}+\mathrm{e}^{\mathrm{i}\frac{2\pi\,(j-\ell)}{N}}\partial_1^{(1)})\kappa_{\ell 0}^{(11)\,*} \\[4pt]
(\partial_0^{(1)}+\mathrm{e}^{\mathrm{i}\frac{2\pi\,(k-j)}{N}}\partial_1^{(1)})(\partial_0^{(2)}+\mathrm{e}^{\mathrm{i}\frac{2\pi\,(j-\ell)}{N}}\partial_1^{(2)})\kappa_{\ell 0}^{(11)\,*} \\[4pt]
(\partial_0^{(2)}+\mathrm{e}^{\mathrm{i}\frac{2\pi\,(k-j)}{N}}\partial_1^{(2)})(\partial_0^{(1)}+\mathrm{e}^{\mathrm{i}\frac{2\pi\,(j-\ell)}{N}}\partial_1^{(1)})\kappa_{\ell 0}^{(11)\,*} \\[4pt]
(\partial_0^{(2)}+\mathrm{e}^{\mathrm{i}\frac{2\pi\,(k-j)}{N}}\partial_1^{(2)})(\partial_0^{(2)}+\mathrm{e}^{\mathrm{i}\frac{2\pi\,(j-\ell)}{N}}\partial_1^{(2)})\kappa_{\ell 0}^{(11)\,*} \\[4pt]
(\partial_0^{(1)}+\mathrm{e}^{\mathrm{i}\frac{2\pi\,(k-j)}{N}}\partial_1^{(1)})(\partial_0^{(1)}+\mathrm{e}^{\mathrm{i}\frac{2\pi\,(j-\ell)}{N}}\partial_1^{(1)})\kappa_{\ell 0}^{(12)\,*} \\[4pt]
(\partial_0^{(1)}+\mathrm{e}^{\mathrm{i}\frac{2\pi\,(k-j)}{N}}\partial_1^{(1)})(\partial_0^{(2)}+\mathrm{e}^{\mathrm{i}\frac{2\pi\,(j-\ell)}{N}}\partial_1^{(2)})\kappa_{\ell 0}^{(12)\,*} \\[4pt]
(\partial_0^{(2)}+\mathrm{e}^{\mathrm{i}\frac{2\pi\,(k-j)}{N}}\partial_1^{(2)})(\partial_0^{(1)}+\mathrm{e}^{\mathrm{i}\frac{2\pi\,(j-\ell)}{N}}\partial_1^{(1)})\kappa_{\ell 0}^{(12)\,*} \\[4pt]
(\partial_0^{(2)}+\mathrm{e}^{\mathrm{i}\frac{2\pi\,(k-j)}{N}}\partial_1^{(2)})(\partial_0^{(2)}+\mathrm{e}^{\mathrm{i}\frac{2\pi\,(j-\ell)}{N}}\partial_1^{(2)})\kappa_{\ell 0}^{(12)\,*} \\[4pt]
(\partial_0^{(1)}+\mathrm{e}^{\mathrm{i}\frac{2\pi\,(k-j)}{N}}\partial_1^{(1)})(\partial_0^{(1)}+\mathrm{e}^{\mathrm{i}\frac{2\pi\,(j-\ell)}{N}}\partial_1^{(1)})\kappa_{\ell 0}^{(21)\,*} \\[4pt]
(\partial_0^{(1)}+\mathrm{e}^{\mathrm{i}\frac{2\pi\,(k-j)}{N}}\partial_1^{(1)})(\partial_0^{(2)}+\mathrm{e}^{\mathrm{i}\frac{2\pi\,(j-\ell)}{N}}\partial_1^{(2)})\kappa_{\ell 0}^{(21)\,*} \\[4pt]
(\partial_0^{(2)}+\mathrm{e}^{\mathrm{i}\frac{2\pi\,(k-j)}{N}}\partial_1^{(2)})(\partial_0^{(1)}+\mathrm{e}^{\mathrm{i}\frac{2\pi\,(j-\ell)}{N}}\partial_1^{(1)})\kappa_{\ell 0}^{(21)\,*} \\[4pt]
(\partial_0^{(2)}+\mathrm{e}^{\mathrm{i}\frac{2\pi\,(k-j)}{N}}\partial_1^{(2)})(\partial_0^{(2)}+\mathrm{e}^{\mathrm{i}\frac{2\pi\,(j-\ell)}{N}}\partial_1^{(2)})\kappa_{\ell 0}^{(21)\,*} \\[4pt]
(\partial_0^{(1)}+\mathrm{e}^{\mathrm{i}\frac{2\pi\,(k-j)}{N}}\partial_1^{(1)})(\partial_0^{(1)}+\mathrm{e}^{\mathrm{i}\frac{2\pi\,(j-\ell)}{N}}\partial_1^{(1)})\kappa_{\ell 0}^{(22)\,*} \\[4pt]
(\partial_0^{(1)}+\mathrm{e}^{\mathrm{i}\frac{2\pi\,(k-j)}{N}}\partial_1^{(1)})(\partial_0^{(2)}+\mathrm{e}^{\mathrm{i}\frac{2\pi\,(j-\ell)}{N}}\partial_1^{(2)})\kappa_{\ell 0}^{(22)\,*} \\[4pt]
(\partial_0^{(2)}+\mathrm{e}^{\mathrm{i}\frac{2\pi\,(k-j)}{N}}\partial_1^{(2)})(\partial_0^{(1)}+\mathrm{e}^{\mathrm{i}\frac{2\pi\,(j-\ell)}{N}}\partial_1^{(1)})\kappa_{\ell 0}^{(22)\,*} \\[4pt]
(\partial_0^{(2)}+\mathrm{e}^{\mathrm{i}\frac{2\pi\,(k-j)}{N}}\partial_1^{(2)})(\partial_0^{(2)}+\mathrm{e}^{\mathrm{i}\frac{2\pi\,(j-\ell)}{N}}\partial_1^{(2)})\kappa_{\ell 0}^{(22)\,*}
\end{bmatrix}.
\tag{110}
$$

Appendix 4: Remaining Quadratic Terms for Mode 0

In Eq. (77), $\frac{1}{2}\hat{\mathbf{R}}(\hat{\mathbf{u}})\hat{\mathbf{u}}$ represents the quadratic terms that cannot be eliminated by the near-identity transformation (38) when modes 1 and $N-1$ undergo a Hopf bifurcation. The only two nonzero entries in matrix $\hat{\mathbf{R}}(\hat{\mathbf{u}})$ are given by

$$[\hat{\mathbf{R}}(\hat{\mathbf{u}})]_{(1,2)} = \begin{bmatrix} 0 & 0 \\ 4\,q_1\,\sin^2\left(\frac{\pi}{N}\right) z_{N-1}^{(1)} & 0 \end{bmatrix}, \quad [\hat{\mathbf{R}}(\hat{\mathbf{u}})]_{(1,N)} = \begin{bmatrix} 0 & 0 \\ 4\,q_1\,\sin^2\left(\frac{\pi}{N}\right) z_1^{(1)} & 0 \end{bmatrix}, \tag{111}$$

where subscripts denote the location of the block in $\hat{\mathbf{R}}(\hat{\mathbf{u}})$, and q_1 gives the value of q at the bifurcation point; cf. (10). Indeed, these quadratic terms correspond to the modes 1 and $N-1$, and they only appear in the dynamics of the $k=0$ mode. In the special case, when $\beta = 0$ and even N the term

$$[\hat{\mathbf{R}}(\hat{\mathbf{u}})]_{(1,\frac{N}{2}+1)} = \begin{bmatrix} 0 & 0 \\ 4\,q_1\,z_{\frac{N}{2}}^{(1)} & 0 \end{bmatrix}, \tag{112}$$

also remains in the equation of the $k=0$ mode due to mode $N/2$.

Appendix 5: Quadratic Near-Identity Coefficients for the Connected Vehicle Example

Equations (83) and (88) contain four nonzero quadratic near-identity coefficients that can be obtained by solving (57) for the car following model:

$$
\begin{aligned}
\psi_{21}^{(111)} =\ & \frac{q_1\,(e^{i\frac{2\pi}{N}}-1)^2}{2\,\Delta}\Big(-\left(2\kappa_{10}^{(21)\,*}-\kappa_{20}^{(21)\,*}\right)\left(4\kappa_{10}^{(21)\,*}-\kappa_{20}^{(21)\,*}\right)\\
& -2\kappa_{10}^{(21)\,*}\left(\kappa_{10}^{(22)\,*}-\kappa_{20}^{(22)\,*}\right)\kappa_{20}^{(22)\,*}+\kappa_{20}^{(21)\,*}\kappa_{10}^{(22)\,*}\left(5\kappa_{10}^{(22)\,*}-3\kappa_{20}^{(22)\,*}\right)\\
& -2\left(\kappa_{10}^{(22)\,*}\right)^2\left(\kappa_{10}^{(22)\,*}-\kappa_{20}^{(22)\,*}\right)\left(2\kappa_{10}^{(22)\,*}-\kappa_{20}^{(22)\,*}\right)\Big),\\
\psi_{21}^{(112)}+\psi_{21}^{(121)} =\ & \frac{-q_1\,(e^{i\frac{2\pi}{N}}-1)^2}{\Delta}\Big(4\kappa_{10}^{(21)\,*}\kappa_{10}^{(22)\,*}+\kappa_{20}^{(21)\,*}\left(\kappa_{10}^{(22)\,*}-\kappa_{20}^{(22)\,*}\right)\\
& -2\kappa_{10}^{(22)\,*}\left(\kappa_{10}^{(22)\,*}-\kappa_{20}^{(22)\,*}\right)\left(2\kappa_{10}^{(22)\,*}-\kappa_{20}^{(22)\,*}\right)\Big),\\
\psi_{21}^{(122)} =\ & \frac{q_1\,(e^{i\frac{2\pi}{N}}-1)^2}{\Delta}\Big(\left(4\kappa_{10}^{(21)\,*}-\kappa_{20}^{(21)\,*}\right)-\left(\kappa_{10}^{(22)\,*}-\kappa_{20}^{(22)\,*}\right)\left(2\kappa_{10}^{(22)\,*}-\kappa_{20}^{(22)\,*}\right)\Big),
\end{aligned}
\tag{113}
$$

where the factor Δ is

$$
\begin{aligned}
\Delta =\ & \kappa_{20}^{(21)\,*}\left(4\kappa_{10}^{(21)\,*}-\kappa_{20}^{(21)\,*}\right)^2 - 16\kappa_{10}^{(22)\,*}\left(\kappa_{10}^{(22)\,*}-\kappa_{20}^{(22)\,*}\right)\left(\kappa_{10}^{(21)\,*}\right)^2\\
& + 4\left(2\left(\kappa_{10}^{(22)\,*}\right)^2-\left(\kappa_{20}^{(22)\,*}\right)^2\right)\kappa_{10}^{(21)\,*}\kappa_{20}^{(21)\,*}-\kappa_{10}^{(22)\,*}\left(5\kappa_{10}^{(22)\,*}-3\kappa_{20}^{(22)\,*}\right)\left(\kappa_{20}^{(22)\,*}\right)^2\\
& + 2\kappa_{10}^{(22)\,*}\left(\kappa_{10}^{(22)\,*}-\kappa_{20}^{(22)\,*}\right)\left(2\kappa_{10}^{(22)\,*}-\kappa_{20}^{(22)\,*}\right)\left(-2\kappa_{10}^{(21)\,*}\kappa_{20}^{(22)\,*}+\kappa_{20}^{(21)\,*}\kappa_{10}^{(22)\,*}\right),
\end{aligned}
\tag{114}
$$

and q_1 gives the value of q at the bifurcation point; cf. (10). We remark that the coefficients $\psi_{21}^{(112)}$ and $\psi_{21}^{(121)}$ do not need to be evaluated individually since (83, 88) only include their sum.

References

Cochelin, B., Damil, N., Potier-Ferry, M.: Asymptotic-numerical methods and Pade approximations for non-linear elastic structures. Int. J. Numer. Methods Eng. **37**(7), 1187–1213 (1994)

Gasser, I., Sirito, G., Werner, B.: Bifurcation analysis of a class of 'car following' traffic models. Phys. D **197**(3–4), 222–241 (2004)

Ge, J.I., Avedisov, S.S., Orosz, G.: Stability of connected vehicle platoons with delayed acceleration feedback. In: Proceedings of the ASME Dynamic Systems and Control Conference, pp. V002T30A006. ASME (2013). Paper no. DSCC2013-4040

Ge, J.I., Orosz, G.: Dynamics of connected vehicle systems with delayed acceleration feedback. Transp. Res. Part C. **46**, 46–64 (2014)

Gendelman, O.V.: Bifurcations of nonlinear normal modes of linear oscillator with strongly nonlinear damped attachment. Nonlinear Dyn. **37**(2), 115–128 (2004)

Georgiades, F., Peeters, M., Kerschen, G., Golinval, J.C., Ruzzene, M.: Modal analysis of a nonlinear periodic structure with cyclic symmetry. AIAA J. **47**(4), 1014–1025 (2009)

Grolet, A., Thouverez, F.: Vibration analysis of a nonlinear system with cyclic symmetry. J. Eng. Gas Turbines Power **133**(2), 022502 (2011)

Haterbouch, M., Benamar, R.: Geometrically nonlinear free vibrations of simply supported isotropic thin circular plates. J. Sound Vib. **280**(3–5), 903–924 (2005)

Helbing, D., Moussaid, M.: Analytical calculation of critical pertubation amplitudes and critical densities by non-linear stability analysis of a simple traffic flow model. Eur. Phys. J. B **69**(4), 571–581 (2009)

Jézéquel, L., Lamarque, C.H.: Analysis of non-linear dynamic systems by the normal form theory. J. Sound Vib. **149**(3), 429–459 (1991)

Kerschen, G., Peeters, M., Golinval, J.C., Vakakis, A.F.: Nonlinear normal modes, Part I: a useful framework for the structural dynamicist. Mech. Syst. Signal Process. **23**(1), 170–194 (2009)

Kuznetsov, Y.: Elements of Applied Bifurcation Theory. Springer, Berlin (2004)

Manevich, L.I., Mikhlin, Y.V.: On periodic solutions close to rectilinear normal vibration modes. J. Appl. Math. Mech. (PMM) **36**(6), 1051–1058 (1972)

Nayfeh, A.H.: On direct methods for constructing nonlinear normal modes of continuous systems. J. Vib. Control **1**(4), 389–430 (1995)

Nayfeh, A.H., Nayfeh, S.A.: On nonlinear modes of continuous systems. J. Vib. Acoustics **116**(1), 129–136 (1994)

Olson, B.J., Shaw, S.W., Shi, C., Pierre, C., Parker, R.G.: Circulant matrices and their application to vibration analysis. Appl. Mech. Rev. **66**(4), 040803 (2014)

Orosz, G.: Connected cruise control: modeling, delay effects, and nonlinear behavior. Vehicle Syst. Dyn. (submitted) (2014)

Orosz, G., Moehlis, J., Bullo, F.: Delayed car-following dynamics for human and robotic drivers. In: Proceedings of the ASME IDETC/CIE Conference, pp. 529–538. ASME (2011). Paper no. DETC2011-48829

Orosz, G., Stépán, G.: Subcritical Hopf bifurcations in a car-following model with reaction-time delay. Proc. R. Soc. **462**(2073), 2643–2670 (2006)

Orosz, G., Wilson, R.E., Stépán, G.: Traffic jams: dynamics and control. Philos. Trans. R. Soc. A. **368**(1928), 4455–4479 (2010)

Orosz, G., Wilson, R.E., Szalai, R., Stépán, G.: Exciting traffic jams: nonlinear phenomena behind traffic jam formation on highways. Phys. Rev. E. **80**(4), 046205 (2009)

Peeters, M., Viguié, R., Sérandour, G., Kerschen, G., Golinval, J.C.: Nonlinear normal modes, Part II: toward a practical computation using numerical continuation techniques. Mech. Syst. Signal Process. **23**(1), 195–216 (2009)

Qin, W.B., Gomez, M.M., Orosz, G.: Stability analysis of connected cruise control with stochastic delays. In: Proceedings of the American Control Conference, pp. 4624–4629. IEEE (2014)

Roose, D., Szalai, R.: Continuation and bifurcation analysis of delay differential equations. In: Krauskopf, B., Osinga, H.M., Galan-Vioque, J. (eds.) Numerical Continuation Methods for Dynamical Systems, Understanding Complex Systems, pp. 359–399. Springer, Berlin (2007)

Rosenberg, R.M.: On nonlinear vibrations of systems with many degrees of freedom. Adv. Appl. Mech. **9**, 155–242 (1966)

Shaw, S.W., Pierre, C.: Normal modes for non-linear vibratory systems. J. Sound Vib. **164**(1), 85–124 (1993)

Shladover, S.E.: Longitudinal control of automotive vehicles in close-formation platoons. J. Dyn. Syst. Meas. Contr. **113**(2), 231–241 (1991)

Slater, J.C.: A numerical method for determining nonlinear normal modes. Nonlinear Dyn. **10**(1), 19–30 (1996)

Szemplinska-Stupnicka, W.: "Non-linear normal modes" and the generalized Ritz method in the problems of vibrations of non-linear elastic continuous systems. Int. J. Non-linear Mech. **18**(2), 149–165 (1983)

Wang, F., Bajaj, A.K.: Nonlinear normal modes in multi-mode models of an inertially coupled elastic structure. Nonlinear Dyn. **47**(1–3), 25–47 (2007)

Zhang, L., Orosz, G.: Designing network motifs in connected vehicle systems: delay effects and stability. In: Proceedings of the ASME Dynamic Systems and Control Conference, pp. V003T42A006. ASME (2013). Paper no. DSCC2013-4081